Investigation of steatosis profiles induced by pesticides using liver organ-on-chip model and omics analysis

Rachid Jellali, Sebastien Jacques, Amal Essaouiba, Françoise Gilard, Franck Letourneur, Bertrand Gakière, Cécile Legallais, Eric Leclerc

Investigation of steatosis profiles induced by pesticides using liver organ-on-chip model and omics analysis

Rachid Jellali [1*], Sebastien Jacques [2], Amal Essaouiba [1], Françoise Gilard [3], Bertrand Gakière [3], Franck Letourneur [2], Cécile Legallais [1], Eric Leclerc [1*]

[1] *Université de technologie de Compiègne, CNRS, Biomechanics and Bioengineering, Centre de recherche Royallieu CS 60319, 60203 Compiègne Cedex, France*
[2] *Université de Paris, Institut Cochin, INSERM, CNRS, F-75014 PARIS, France*
[3] *Plateforme Métabolisme Métabolome, Institute of Plant Sciences Paris-Saclay (IPS2), CNRS, INRA, Univ. Paris-Sud, Univ. Evry, Univ. Paris-Diderot, Univ. Paris Saclay, Bâtiment 630 Rue Noetzlin, 91192, Gif-sur-Yvette cedex, France*

* Corresponding author
Rachid Jellali: rachid.jellali@utc.fr
Eric Leclerc: eric.leclerc@utc.fr

Highlights

- Rat liver organ-on-chip model was used to study pesticides toxicity

- The model was exposed to DDT, permethrin and their mixtures at 15 and 150 μM

- Transcriptome and metabolome profile showed a dose-dependent effect

- Liver steatosis, inflammation and cell death were common signature for high-doses

- Mixture of DDT and PMT led to additive and increased effects

Abstract

Several studies have reported a correlation between pesticides exposure and metabolic disorders. Dichlorodiphenyltrichloroethane (DDT) and permethrin (PMT), two pesticides highly prevalent in the environment, have been associated to dysregulation of liver lipids and glucose metabolisms and none-alcoholic fatty liver disease (NAFLD). However, the effects of DDT/PMT mixtures and mechanisms mediating their action remain unclear. Here, we used multi-omic to investigate the liver damage induced by DDT, PMT and their mixture in rat liver organ-on-chip. Organ-on-chip allow the reproduction of *in vivo*-like micro-environment. Two concentrations, 15 and 150μM, were used to expose the hepatocytes for 24h under perfusion. The transcriptome and metabolome analysis suggested a dose-dependent effect for all conditions, with a profile close to control for pesticides low-doses. The comparison between control and high-doses detected 266/24, 256/24 and 1349/30 genes/metabolites differentially expressed for DDT150, PMT150 and Mix150 (DDT150/PMT150). Transcriptome modulation reflected liver inflammation, steatosis, necrosis, PPAR signaling and fatty acid metabolism. The metabolome analysis highlighted common signature of three treatments including lipid and carbohydrates production, and a decrease in amino acids and krebs cycle intermediates. Our study illustrates the potential of organ-on-chip coupled to multi-omics for chemical risk assessment and provides tools to move from studies based on animal experiments.

Keywords: steatosis, pesticides, liver, organ on chip, transcriptomic, metabolomic

Investigation of steatosis profiles induced by pesticides using liver organ-on-chip model and omics analysis

Rachid Jellali [1*], Sebastien Jacques [2], Amal Essaouiba [1], Françoise Gilard [3], Franck Letourneur [2], Bertrand Gakière [3], Cécile Legallais [1], Eric Leclerc [1*]

1 Université de technologie de Compiègne, CNRS, Biomechanics and Bioengineering, Centre de recherche Royallieu CS 60319, 60203 Compiègne Cedex, France
2 Université de Paris, Institut Cochin, INSERM, CNRS, F-75014 PARIS, France
3 Plateforme Métabolisme Métabolome, Institute of Plant Sciences Paris-Saclay (IPS2), CNRS, INRA, Univ. Paris-Sud, Univ. Evry, Univ. Paris-Diderot, Univ. Paris Saclay, Bâtiment 630 Rue Noetzlin, 91192, Gif-sur-Yvette cedex, France

* Corresponding author
Rachid Jellali: rachid.jellali@utc.fr
Eric Leclerc: eric.leclerc@utc.fr

Abstract

Several studies have reported a correlation between pesticides exposure and metabolic disorders. Dichlorodiphenyltrichloroethane (DDT) and permethrin (PMT), two pesticides highly prevalent in the environment, have been associated to dysregulation of liver lipids and glucose metabolisms and none-alcoholic fatty liver disease (NAFLD). However, the effects of DDT/PMT mixtures and mechanisms mediating their action remain unclear. Here, we used multi-omic to investigate the liver damage induced by DDT, PMT and their mixture in rat liver organ-on-chip. Organ-on-chip allow the reproduction of *in vivo*-like micro-environment. Two concentrations, 15 and 150μM, were used to expose the hepatocytes for 24h under perfusion. The transcriptome and metabolome analysis suggested a dose-dependent effect for all conditions, with a profile close to control for pesticides low-doses. The comparison between control and high-doses detected 266/24, 256/24 and 1349/30 genes/metabolites differentially expressed for DDT150, PMT150 and Mix150 (DDT150/PMT150). Transcriptome modulation reflected liver inflammation, steatosis, necrosis, PPAR signaling and fatty acid metabolism. The metabolome analysis highlighted common signature of three treatments including lipid and carbohydrates production, and a decrease in amino acids and krebs cycle intermediates. Our study illustrates the potential of organ-on-chip coupled to multi-omics for chemical risk assessment and provides tools to move from studies based on animal experiments.

Introduction

Pesticides are extensively used all over the world to provide high agricultural productivity and control of vector-borne diseases (Ghisari et al., 2015). As a result, pesticide residues are present in the human food supply, soil, water, atmosphere and agricultural product (Ghisari et al., 2015; Rizzati et al., 2016). Nowadays, exposure to pesticides is a widely recognized concern for human biosafety. Permethrin (PMT, 3-phenoxybenzyl (±) *cis/trans*-3-(2,2-dichlorovinyl)-2,2-dimethylcyclopropane-1-carboxylate), the most popular pyrethroid, is a broad-spectrum insecticide used worldwide to treat a wide range of insects in agriculture, public health, and homes (Willemin et al., 2016; Xiao et al., 2017). Several studies reported the presence of significant levels of PMT and its metabolites in fruits, vegetables, breast milk and human urine and hair (Fedeli et al., 2017; Béranger et al., 2018; Xiang et al., 2018). Dichlorodiphenyl-trichloroethane (DDT) is an organochlorine insecticide that has been largely used to control agricultural pest and eradicate malaria, typhus and other diseases (Harrada et al., 2016). Despite its interdiction in most countries since 1970, DDT and its metabolites remain in the environment due to their low degradability and bio-accumulative properties (Jin et al., 2014). Additionally, DDT is still used in some countries for malaria control and for dicofol production (Peng et al., 2020; Huq et al., 2020). Consequently, DDT are still consistently found in soil, food, seawater, porewater, human, and animal samples (Russo et al., 2019; Song et al., 2019; Peng et al., 2020).

PMT and DDT, with its metabolite DDE (dichlorodiphenyl- dichloroethylene), was associated to several harmful effects in animals and humans. Both pesticides cause a variety of toxicities in immune, nervous, endocrine and reproductive systems (Harrada et al., 2016; Wang et al., 2016; Willemin et al., 2016; Jellali et al., 2018; Huq et al., 2020). As the primary target of chemical pollutants, the liver is severely affected by exposure to pesticides. PMT and DDT exposure increases hepatic oxidative stress and liver weight, and causes hepatic cell death (Kostka et al., 2000; Wang et al., 2016; Harrada et al., 2016; Jellali et al., 2018a). DDT and its metabolites are also associated with high liver cancer risk (VoPham et al., 2017). In the last years, accumulating evidences suggest an association between PMT, DDT (with DDE) and diseases related to metabolic disorders including obesity, dysregulation of lipid and glucose metabolisms, insulin resistance, none-alcoholic fatty liver disease (NAFLD), and type 2 diabetes (Howell et al., 2015; Liu et al., 2017a; Xiao et al., 2017; Yang and Park 2018; Xiao et al., 2018; Yang et al., 2019; Wu et al., 2019; He et al., 2020; Hu et al., 2020). In particular, NAFLD is currently a major health concern, with 25% of adults affected worldwide (Yang et

al., 2019). Al Eryani et al., reported that pesticides were among the chemicals most frequently associated with NAFLD in rodents toxicology studies (Al Eryani et al., 2015). However, although the association between pesticides (including PMT and DDT) and metabolic disorders was established, the underlying mechanisms for how pesticides would lead these disorders have not yet been fully clarified. Furthermore, there is a serious lack of information on the toxicity of PMT and DDT mixtures.

Muti-omics studies including transcriptomics, metabolomics and proteomics represent a promising tool to investigate pesticides toxicity and to elucidate the mechanisms and pathways by which these chemicals manifest their toxicities (Brockmeier et al., 2017; Canzler et al., 2020). Metabolomics, or the study of the metabolome, focuses on the detection and identification of low molecular weight (< 1500 Da) compounds produced by chemical reactions taking place in cells or the whole organism (Canzler et al., 2020). It makes it possible to identify both variations in the composition of the culture medium or cellular fluid, and metabolic changes occurring after exposure to pesticides (Song et al.,2016). Transcriptomics consists of analysing all species of transcripts, including mRNAs, non-coding RNAs and small RNAs, and can provide a complete analysis of the hereditary material in a biological system (Wang et al., 2009; Prot et al., 2012). Transcriptional profiling can be employed to detect changes in gene expression following exposure to pesticides. These changes representing early and mechanistically relevant cellular events can potentially provide valuable information for understanding the mode of action of pesticides (De Abrew et al., 2015; Joseph 2017). In last years, metabolomics and/or transcriptomics have been widely used to investigate effects of pesticides and investigate their mechanisms of action (Liang et al., 2013; Roede et al., 2014; Jeffries et al., 2015; Zuluaga et al., 2016; Krauskopf et al., 2017; Morales-Prieto et al., 2018; Jellali et al., 2018b; Hu et al., 2020). However, to our knowledge, there is no study integrating metabolomics and transcriptomics to investigate effects of DDT, PMT and their mixture on liver cells.

In pesticides toxicology research, most commonly, animal models or *in vitro* 2D cell cultures in Petri dishes are employed. However, the animal models lose their relevance when extrapolating the results to humans and 2D culture are poorly predictive of human in vivo metabolism and toxicity (Merlier et al., 2017, Štampar et al., 2020). In recent year, 3D cultures, co-cultures and organ-on-chip, which more adequately resemble in vivo cell behavior, were increasingly used in toxicological studies (Aggerbeck and Blanc 2018). Of those models,

dynamic organ-on-chip culture seems to be one of the best-suited methods for reproducing the behavior of an organ or a group of organs, the controlled physiological micro-environment and *in vivo* cellular metabolic responses (Merlier et al., 2017; Kimura et al., 2018). Our group has proposed organ-on-chip solutions coupled to omics analysis and presented new insight in liver metabolism (Jellali et al., 2016a), crosstalk and synergy between different organs (Choucha-Snouber et al., 2013; Bricks et al., 2014; Essaouiba et al., 2020), as well as predictive toxicology by identifying biomarkers and metabolic signatures in response to drugs and pesticides (Prot et al., 2012, Choucha- Snouber et al., 2012, Jellali et al., 2018a, 2018b). In the present investigation, we describe the changes in metabolomics and transcriptomics profiles of rat liver-on-chip exposed to PMT, DDT and their mixture. Our study highlighted steatosis-associated biomarkers of exposure to these chemicals.

2. Materials and methods

2.1. Biochip and fluidic platform

The biochips and fluidic platform have already been detailed in our previous work (Baudoin et al., 2012; Jellali et al., 216b). The microfluidic device (liver biochip) was manufactured with two polydimethylsiloxane layers (PDMS, Sylgard 184 kit, Dow Corning), sealed by reactive air plasma treatment (plasma cleaner, Harrick Plasma). The microstructures in bottom layer define several cell cultures chambers and microchannels (depth of 100 µm, Fig.S1, supplementary file). The top layer, with a reservoir (depth of 100 µm), includes an inlet and outlet for culture medium perfusion (Fig.S1, supplementary file 1).

For dynamic culture, the biochips were connected to our IDCCM device (Integrated Dynamic Cell Cultures in Microsystems, Fig.S1, supplementary file1). The IDCCM device is a polycarbonate platform (with the conventional format of 24-well plate) manufactured by molding injection. The biochips are connected at the bottom of the IDCCM device by a simple series of connectors. Each biochip is connected between two wells (volume of 2 mL per well), allowing the parallelization of 12 biochips. The perfusion was performed using peristaltic pump connected to the cover of the IDCCM device by PTFE tubes (Fig.S1, supplementary file 1).

2.2. Culture medium and chemical reagents

The primary hepatocytes seeding medium (adhesion phase) was composed of William's E medium (Gibco) supplemented with 10% fetal bovine serum (FBS, Gibco), GlutaMAX (Gibco) at 10 mM,100 units/mL of penicillin and 100 mg/mL of streptomycin (Gibco). In dynamic culture phase, the hepatocytes were cultivated in culture medium: William's E medium supplemented with 100 units/mL of penicillin / 100 mg/mL of streptomycin, GlutaMAX at 10 mM, 1% non-essential amino acids (Gibco), 3% Bovine Serum Albumin (BSA, Sigma-Aldrich), 1% Insulin-Transferrin-Selenium ITS-100X (PanBiotech), 0.1 μM Dexamethasone (Sigma-Aldrich), 0.5 mM ascorbic acid 2-phosphate (from magnesium salt n-hydrate, Sigma-Aldrich) and 20 mM HEPES (Gibco).

p,p'-dichlorodiphenyltrichloroethane (DDT,) and Cis-Permethrin (3-phenoxybenzyl (1RS)-cis-3-(2,2-dichlorovinyl)-2,2- dimethylcyclopropane carboxylate, PMT) were purchased from Sigma-Aldrich and Supelco Analytical, respectively. Solutions stock of both pesticides (at different concentrations) were prepared in dimethyl sulfoxide (DMSO, Sigma-Aldrich). Further dilutions in culture medium were realized to achieve the final concentrations of expositions. The final concentration of DMSO in the culture medium did not exceed 0.2% (v/v) that did not affect cell viability and culture medium with 0.2 % of DMSO was used as control.

2.3. Primary rat hepatocytes culture in microfluidic biochip

Primary rat hepatocytes were isolated from 5-week-old male Sprague-Dawley rats (Janvier Labs, France) using the two-step collagenase protocol based on the protocol of Seglen (1973). The details of the hepatocytes extraction protocol are given in our previous work and in supplementary file 2 (Jellali et al., 2018a). Rats were housed in ventilated, humidity and temperature-controlled rooms with a 12/12-h light/dark cycle, with food and water ad libitum. All procedures were performed with the approval of the Veterinary Authorities of France in accordance with the European Communities Council Directive of 22 September 2010:63/UE. This study was approved by the ethics committee of the Université de Technologie de Compiègne.

The biochips, IDCCM device and tubing were sterilized by autoclaving and dried in an oven. The biochips were connected to the IDCCM device, coated with rat tail type I collagen

(Corning®, 300 µg/mL in phosphate- buffered saline: PBS, Gibco) and incubated at 37°C in an atmosphere supplied with 5% CO_2. After 1h, the collagen solution was washed using the seeding medium and the freshly isolated hepatocytes ($5.5x10^5 \pm 0.2x10^5$ cells/biochip) loaded into the biochips via IDCCM inlet ports using a micropipette tip. Each well of IDCCM box was completed by 2 ml of seeding medium. After 24 h (37°C, 5% CO2) of static conditions to promote cell adhesion, the seeding medium was replaced by the culture medium, the IDCCM device connected to the peristaltic pump and the perfusion was started (25 µL/min). Finally, the pesticides solutions were added and the experiment was continued for 24 hours in dynamic conditions. At the end of the experiment, the culture medium and cells were collected for analysis. The detailed experimental procedure is shown in Fig.1A.

The pesticides concentrations were selected based on the literature data (Leibold and Schwarz 1992; Zucchini-Pascal et al., 2012; Willemin et al., 2015; Willemin et al., 2016; Yang et al., 2019). In this work, DDT and PMT were supplied at 15 (DDT15 and PMT15) and 150 µM (DDT150 and PMT150). We also tested mixtures of DDT and PMT at 15 (Mix15) and 150 µM (Mix150). Although the concentrations of DDT and PMT used were higher than reported human cases, both pesticides are very lipophilic molecules and can accumulate in hydrophobic tissue, such as in adipose tissue (Yang et al., 2019).

2.3. Cell viability and functionality

Cell counting was performed on a Malassez cell following cell detachment with trypsin-EDTA (Fisher Scientific) and the viability was quantitatively analyzed using trypan blue staining. The productions of albumin and urea were measured using ELISA assays (Rat Albumin ELISA quantification set, Bethyl) and QuantiChromTM Urea Assay Kit (DIUR-500), respectively (detailed protocols are provided in supplementary file 2).

For statistical analysis, one-way ANOVA combined with Dunnett's test was performed using GraphPad Prism 8 software (State College, USA). A P value less than 0.05 was considered as statistically significant.

2.4. Transcriptomic analysis

Total RNA was extracted using the Nucleospin® RNA XS isolation kit (Macherey-Nagel EURL, Hoerdt, France). After validation of the RNA quality with Bioanalyzer 2100 (using Agilent RNA6000 nano chip kit), 500 ng of total RNA is reverse transcribed following the GeneChip® WT Plus Reagent Kit (Affymetrix). Briefly, the resulting double strand cDNA is used for in vitro transcription with T7 RNA polymerase (all these steps are included in the WT cDNA synthesis and amplification kit of Affymetrix). After purification according to Affymetrix protocol, 5.5 ug of the cDNA obtained are fragmented and biotin labelled using Terminal Transferase (using the WT terminal labelling kit of Affymetrix). cDNA is then hybridized to GeneChip™ Rat Transcriptome Array 1.0 (RTA 1.0.) (Affymetrix) at 45°C for 17 hours. After overnight hybridization, chips are washed on the fluidic station FS450 following specific protocols (Affymetrix) and scanned using the GCS3000 7G.

The scanned images are then analyzed with Expression Console software (Affymetrix) to obtain raw data (.cel files) and metrics for Quality Controls. The observations of some of these metrics and the study of the distribution of raw data show no outlier experiment. Robust Multichip Algorithm (RMA) normalization was realized using R and normalized data were subjected to statistical tests. To find differentially expressed genes (DEGs), a t-test was performed using MeV 4.9 software.

The gene lists selected by the t-test (P value of less than 0.05) were filtered according to the fold change in order to conserve only the genes with a fold change of more than 1.2 (up-regulated) or less than -1.2 (down-regulated). The corresponding lists of DEGs were fed to Ingenuity Pathway Analysis (IPA) to obtain biological functions, top network and gene ID. The ISMARA webserver (https://ismara.unibas.ch/mara/) was used for Motif Activity Response Analysis (MARA, Balwierz, et al., 2014).

2.5. Metabolomic analysis

Metabolomic analysis was performed with the culture medium collected at the end of each step using gas chromatography (Agilent 7890B) coupled to mass spectrometry (Agilent 5977A, GC-MS). The column was a Rxi-5SilMS from Restek (30 m with a 10 m Integra-Guard column - ref 13623-127). Sample preparation and metabolite extraction were performed

according to our previous work (Jellali et al., 2018a). All the GC-MS injection and analysis steps were carried out as described in Fiehn et al., (Fiehn 2006; Fiehn et al., 2008). The data files obtained were analyzed using AMDIS software (http://chemdata.nist.gov/mass-spc/amdis/). Peak areas were determined using Masshunter Quantitative Analysis (Agilent) and normalized to ribitol. Metabolite contents are expressed in arbitrary units. The complete protocols for the metabolite extraction and samples injection are detailed in supplementary file 2.

The metabolomic multivariate data analysis was performed using XLSTAT.2016 software (Addinsoft) and MetaboAnalyst 4.0 (Chong et al., 2018). Firstly, unsupervised principal component analysis (PCA) was performed to identify the similarity or the differences between sample profiles and to assess the clustering behavior between groups. Secondly, orthogonal projections to latent structures discriminant analysis (OPLS-DA) was applied to get the maximum separation between control and treated groups, and to explore the variables that contributed to this separation. The quality of OPLS-DA model was evaluated by the R^2Y (fitting degree) and Q^2 (prediction parameter) values. To determine the best discriminators metabolites, the loading from OPLS-DA was constructed by plotting the modelled covariance p[1] on the x- axis and the modelled correlation p(corr)[1] on the y- axis (S- plot). Variables with higher absolute value of correlation (p(corr) > 0.6) represent possible discriminating metabolites (those with higher p[1] values have a larger impact on the variance between the groups) (Bervoets et al., 2014). The significant metabolites were confirmed using variable importance in the projection value (VIP > 1) and Student's *t*-test (P < 0.05). Finally, MetaboAnalyst software were used to integrate metabolomics and transcriptomics data.

3. Results

3.1. Morphology and cell functionality

The hepatocytes cultures were performed over 72 h, including 24 h of static adhesion and 48 h of perfusion. After static phase, the cells were successfully adhered in bottom of biochips. The number of counted cells was about of $4.7 \times 10^5 \pm 0.5 \times 10^5$ cells/biochip. The hepatocyte morphologies at the end of the experiments (24 h of exposure) are presented in Fig.1B and Fig.S2 (supplementary file 1). As shown in Fig.S2, the control and the biochips treated with 15 µM of DDT and 15 µM of PMT (DDT15 and PMT15) presented similar morphologies. The

hepatocytes formed homogeneous and confluent tissue on the microchambers and microchannels bottom surface. By contrast, at DDT150, PMT150, Mix15 and Mix150, the hepatocytes were less dense and cell-free areas were observed in the biochips (Fig.1B and Fig.S2, supplementary file 1). Furthermore, the cell-free areas were more important in the biochip exposed to Mix150. The morphological observations were confirmed by cell counting (Fig.1C). Indeed, the number of collected living cells was of $4.1\pm0.23\text{x}10^5$, $3.8\pm0.45\text{x}10^5$, $3.9\pm0.38\text{x}10^5$, $3\pm0.45\text{x}10^5$, $3.05\pm0.35\text{x}10^5$, $3.1\pm0.31\text{x}10^5$ and $2.1\pm0.13\text{x}10^5$ cells in biochip CT, DDT15, PMT15, Mix15, DDT150, PMT150 and Mix150, respectively.

The hepatocytes functionality was illustrated by albumin and urea production (Fig.1C and Fig.S3 in supplementary file 1, respectively). As shown in Fig.1C, albumin production was about 800-900 $ng/h/10^6$ cells. However, we did not detect any significant effect of pesticides expositions on albumin. For urea production, a significant increase was observed when hepatocytes were exposed to Mix150 (15 ± 2.2 $\mu g/h/10^6$ cells vs. 8 ± 1.1 $\mu g/h/10^6$ cells for control). For all other exposed biochip, the urea production was close to control.

3.2. Transcriptomic analysis

PCA and supervised PLS-DA were performed on transcriptomic data to acquire an overview of variations among the groups. The PCA analysis could not sufficiently separate the groups (Fig.S4A, supplementary file 1). The PLS-DA analysis applied to the dataset led to separation between two groups, as shown in Fig.2A and Fig.S4B (supplementary file 1). The first group includes the control biochips and the samples exposed to DDT15, PMT15 and Mix15, whereas the second group consists of biochips exposed to high pesticides doses. These results were confirmed by PLS-DA presented in Fig.2B (control vs. high-dose) and Fig.S4C (control vs. low-dose).

The separation between the high-dose groups and the control, and the overlap between low-dose and control groups suggested that the effects caused PMT, DDT and PMT/DDT mixtures are dose-dependent. However, as shown in the heatmap in Fig.2C, PMT15, DDT15 and Mix15 presented transcriptomic profiles very close to control. As a result, thereafter, we treated only high-dose versus control groups to investigate pesticides effects and carry out discussions.

3.2.1. DDT Profile

The statistical comparison of the control versus DDT150 revealed 266 differentially expressed genes (DEGs) with a *P* value below 0.05 and a fold change (FC) of ±1.2 (127 downregulated and 139 upregulated, Fig.3A and supplementary file 3). Among them, the top 5 upregulated genes were *Slc25a4* (mitochondrial ADP/ATP transport), *Pla2g7* (coding for a phospholipase that hydrolyze phospholipids into fatty acids and other lipophilic molecules), *Scd2* (involved in the fatty acid biosynthesis), *Hmgn2* (opening chromatin process) and *Cxcl10* (pro inflammatory cytokine). The top 5 downregulated genes were *Bdh1* (3-Hydroxybutyrate Dehydrogenase-1, 3-hydroxybutyrate is one of the major ketone bodies produced during fatty acid catabolism), *Diaph3* (involved in actin remolding), *Cyp3a5/7* (xenobiotic metabolism), *Pemt* (involved in the production of phosphatidylcholine and of phospholipid in liver), *Cyp17a1* (involved in the corticoid and androgen biosynthesis).

The pathways extracted by IPA analysis are summarized in Table 1 (full analysis presented in supplementary file 3). The top 5 canonical pathways highlighted by IPA were the glutathione mediated detoxification (*Gstt2/Gstt2b*, *Gsta2*, *Mgst2*, *Ggh*), the proline biosynthesis/arginine degradation (*Pycrl, Pycr1*), the inhibition of the RXR function (*Gstt2/Gstt2b*, *Gsta2*, *Il18*, *Aldh1l2*, *Scarb1*, *Mgst2*, *Nr1i3*, *Fabp5*, *Cyp4a11*) and the tryptophan degradation (*Haao*, *Ehhadh*, *Hadh*). The top tox function appeared to be the liver steatosis (20 hits), the liver inflammation (14 hits) and liver necrosis (9 hits). Finally, the potential upstream regulators were *Ucp1* (mitochondrial process), *Srebf1* (sterol regulation) and IFNB1 (interferon).

In order to complete the IPA analysis, we performed a second analysis using the microarray dataset with the ISMARA processing. The comparison of the biochip control versus the DDT150 treated conditions led to extract 46 transcription factors (TFs) that were differentially activated (z_value above 1, supplementary file 4). Among them *Hnf4a*, *Hnf4g*, *Ahr* and *Essra* were over activated in control whereas *Esr1* was over activated in DDT150. In the top ten TFs, we extracted the over activation of *Max*, *Yy1*, *Nfia*, *Mxi1*, *Atf4*, *Hic2* in the control biochip. The *Meis3*, *Tfdp1*, *Pml*, *Hoxb7* genes presented an over activity in the DDT150 conditions. Their targets are presented in Table 2 (the full target is given in supplementary file 5). They included important liver markers (*Hnf3*, urea cycle), lipid, carbohydrates and insulin

regulation. Response to inflammation processes (*Nfkb*, *Ifn*, *Tgfb*, p53, GSH) and liver regeneration (*Tgfb*) were also extracted consistently with IPA analysis.

3.2.2. PMT profile

The comparison of the control versus PMT150 are presented in supplementary file 6. The differential analysis led to identify 256 DEGs ($P < 0.05$ and FC ±1.2) between the two conditions (Fig.3A and supplementary file 6). Among them, the top 5 upregulated genes were *Cyp4a11* (metabolism of fatty acid), *Pck1* (gluconeogenesis regulation), *Hmgn2* (opening chromatin process) and *Ehhadh* (beta-oxidation pathway), *Slc34a2* (phosphate transport). The top 5 downregulated genes were *Diaph3*, *Akr1b10* (regulation of lipid production/ lipid degradation), *Defb1* (β defensing-1), *Cyp17a1*, *Cyp3a5/7*. The list of DEGs were then processed using IPA. The top canonical pathways identified were the glycogen biosynthesis (*Gbe1*, *Gys2*), the inhibition of the RXR (8 hits), fatty acid β-oxidation (3 hits) and adipogenesis pathway (6 hits). Regarding the tox function / tox list, the liver steatosis (*Acaca*, *Acadm*, *Cyp4a11*, *Ehhadh*, *Fabp5*, *Fgf21*, *Lpin1*, *Mat1a*, *Mthfr*, *Nr1i3*, *Pck1*, *Prkab1*), liver cirrhosis (*Fbln1*), CAR/RXR activation (*Nr1i3*, *Mdm2*, *Pck1*) and fatty acid metabolism (*Iws1*, *Ehhadh*, *Cyp4a11*, *Acadm*, *Hadh*) appeared among the ''Top pathways" highlighted. The potential upstream regulators included *Ucp1* (mitochondrial process), *Rxrg* (co activator of PPAR, VDR, LXR receptors), *Srebf1* (sterol regulation), *Ppara* (lipid carbohydrates homeostasis) and *Mlxipl* (I activates, in a glucose-dependent manner, the carbohydrate response element (ChoRE) motifs in the promoters of triglyceride synthesis genes). The top pathways and the detailed IPA analysis are presented in Table 1 and supplementary file 6, respectively.

The comparison of the biochip control with the PMT150 treated biochip using ISMARA led to extract 65 transcription factors that were differentially activated (z_value above 1, supplementary file 4). Among them, *Hnf4a*, *Cebpe*, *Cebpb* were over activated in control whereas *Nanog*, *Fos*, *Rarg*, *Esr1*, *Esr2* were over expressed in PMT150. In the top ten, we extracted the over activation of *E2f1*, *Zfp110*, *Max*, *Gabpa*, *Chd2*, *Hsf2* in the control biochip. The *Tgif1*, *Pou1f1*, *Zeb1*, *Mta3* genes presented an over activity in the PMT conditions. Their targets related to liver process and to potential pesticides liver toxicity are presented in Table 3 (the full target is presented in supplementary file 7). The targets included liver marker (*Hnf3b*), lipid and carbohydrates process, and more specifically RNA processes.

3.2.3. Mixture profiles

The differential analysis Mix150 vs CT led to a huge difference between the treated and control conditions, as far as up to 1349 DEGs were extracted ($P < 0.05$ and FC ±1.2, Fig.3A, list of genes in supplementary file 8). Among these DEGs, 788 genes were upregulated and 561 genes were downregulated (Fig.3A). The top 5 upregulated genes were *Pck1*, *Hmgm2*, *Cyp4a11*, *Slc15a1* (peptide transport), *Ggh* (glutamate derived metabolism). The top 5 downregulated genes were *Inkbe* (TGFβ related protein), *Fgf21*, *Fabp5* (fatty acid uptake, transport, metabolism), *Cyp3a5/7*, *Apof* (cholesterol transport regulation).

The IPA pathways analysis revealed the fatty acid β-oxidation III (*Eci33*, *Eci2*, *Ehhadh*, *Eci1*), MAPK signaling (13 hits), TGFβ signalling (15 hits), tryptophan metabolism (6 hits) and estrogen receptor signaling (18 hits) among the top modulated canonical pathways (Table 4 and supplementary file 8). The top 4 tox function were related to liver necrosis and cell death (up to 26 hits). Liver steatosis, liver inflammation, gene regulation by peroxisome Proliferators via *Pparα* and *Tgf-β* signaling were also extracted as top tox function /tox list, with 41 and 40, 17 and 16 hits, respectively. The top potential upstream regulators proposed by IPA were miR-16-5p, *Hnf4a*, *Ppara*, mir-30c-5p. All pathways extracted by IPA are presented in supplementary file 8.

Using ISMARA processing (applied to CT and Mix150 dataset) we extracted 106 transcription factors that were differentially activated (z_value above 1, supplementary file 4). Among them *Foxa1_Foxa2*, *Foxa3*, *Hnf4a*, *Hnf4g*, *Ahr*, *Cebpe*, *Cebpb*, *Cebpa*, *Pparg_rxr*, *Nr1h2* (*Lxr*) were over activated in biochip CT, whereas *Nr2f2*, *Stat2*, *Stat6* were over expressed in Mix150 conditions. In the top ten, we extracted the over activation of the *Max*, *Maz*, *Mta3*, *Atf4* in the control biochip. The *Chd1*, *Zfx*, *Mecp2*, *Nrf1*, *Sp1*, *Irf7* genes presented an over activity in Mix150. The top ten TFs targets related to liver process and to potential pesticides toxicity are presented in table 4 (the full target is given in supplementary file 9).

3.2.4. Cross link between the treatment and specific profiles

To complete the analysis, we crossed the DEGs lists in order to extracted common and specific signatures. As shown in Fig.3B, the Venn diagram representation revealed that 75, 111, 71 and 11 genes were common to the three conditions, DDT150/Mix150, PMT150/Mix150 and

DDT150/PMT150, respectively. The number of genes specific to each exposure condition were of 1092, 69 and 99 for Mix150, DDT150 and PMT150, respectively (full Venn diagram analysis with genes names is provided in supplementary file 10). The correlation matrix performed using the transcriptomic dataset confirms the high similarity between Mix150/DDT150 (correlation coefficient, CC = 0.60) when compared to Mix150/PMT150 (CC = 0.37) and PMT150/DDT150 (CC = 0.15, Fig.3C).

The 75 genes common to three conditions (DDT150, PMT150 and Mix150) are involved in glutathione metabolism and ROS detoxification (*G6pd*, *Gstt2*, *Gstt2b*, *Mgst2*, *Aqp8*), fatty acids, lipids, steroids metabolisms and PPAR signaling (*Cyp4a11*, *Cyp17a1*, *Ehhadh*, *Hadh*, *Fabp5*, *Acaca*, *Tkfc*, *Lpin1*, *Asah2*). They also included inflammation pathway such as TGFb signaling (2 hits), cytokine receptor pathway (4 hits) and their targets (*Stat2*), some genes related to cell remolding (*Cd59*, *Cttnbp2*, *Arhgef2*) and carbohydrates (*Gbe1*, *Tkfc*, *Acaca*, supplementary file 10). Concerning the common genes modulated by DDT150 and Mix150 (111 genes), the profile included cell necrosis, cytokine and inflammation markers (*Irf3*, *Cxcl10*, *Fas*, *Ifnar1*, *Ifngr1*, *il18*, *Inhbc*, *Ripk1*, *Slc25a4*, *Map2k4*), insulin resistance (*Pck2*, *Pten*, *Rps6ka3*, *Trib3*), AMPK signaling (*Adipor2*, *Pck2*, *Fasn*), cholesterol metabolism (*Lrpap1*) and glycine metabolism (*Agtx*, *Gcat*). Finally, the profile of common genes to PMT150 and Mix150 are related to WNT signaling (*Fzd5*, *Gsk3b*, *Myc*), inflammation (*Nfkbiz*, *Tnfrsf1b*, *il17rc*) and insulin resistance (*Pklr*, *Pck1*, *Gsk3b*).

The 69 specific genes of DDT150 treatment included gene related to cell death such as the necrosis (*Cflar*, *Eif2ak2*, *Tlr4*, *Nfkb*, *Myd88*) and autophagy markers (*C2orf72*, *Cflar*, *Rps6kb1*, *Ddit4*). In parallel, the specific genes of PMT150 included more particularly genes related to RNA transport and ribosomes (*Rpl3,4,24,30,32,36a,511*, *Nup43*, *Pnn*) and insulin resistance (*Agt*, *Gys2*, *Prkab1*, *Srebf1*). The mixture of the two pesticides (Mix150) have 1092 specific genes (associated pathways in supplementary file 10).

3.3. Metabolomic profiling

Unsupervised PCA was performed on the GC-MS datasets to compare the metabolic profiles of biochips exposed to pesticides and control. PCA score plots of four analysis (all samples; DDT150 vs. DDT15 vs. CT; DDT150 vs. DDT15 vs. CT and DDT150 vs. DDT15 vs. CT, Fig.S5) showed clear separation between control and biochips exposed to high doses.

Contrary, no obvious separation was observed for control and low pesticides doses. The similarity of biochips treated with low doses and control group was confirmed by the heatmap presented in Fig.S6. consequently, as for transcriptomic data, we treated only high-dose versus control groups to investigate pesticides effects.

OPLS-DA was then applied to data of control and samples treated with pesticides high-dose (that is, CT vs. DDT150, CT vs. PMT150 and CT vs. Mix150). In the OPLS-DA score plot of the three analysis (Figs. 4A, 4B and 4C), pesticides-treated samples were clearly separated from the control group. The OPLS-DA models fitted well the data and showed good predictability ($R^2 = 0.83$, $Q^2 = 0.71$ [DDT150], 0.94, 0.87 [PMT150] and 0.97, 0.93 [Mix150]). To extract the biomarkers, the S-plot from OPLS-DA was plotted using the modelled covariance p[1] and the modelled correlation p(corr)[1] (Figs. 4D, 4E and 4F). When compared to control, the DDT150 exposure led to the modulation of 24 metabolites ($P < 0.05$, Fig.5A). The resulting heatmap and full statistical analysis are shown in Fig.5C and supplementary file 11, respectively. We found an increase in benzoic acid, putrescine, lipid and fatty acids (palmitic, decanoic and octanoic acids), several carbohydrates, their derivatives and glycolysis derivatives (fructose, tagatose, sorbitol and glucaric, glyceric, threonic and pyruvic acids) and amino acids such as arginine, threonine and tyrosine. In parallel, the levels of cysteine, histidine, allantoin (uric acid oxidation) and 2-hydroxybutyric (byproduct of glutathione synthesis), aspartic, citric, and glucuronic acids were decreased.

The PMT150 treatments were associated to the modulation of 24 metabolites (Fig.5A). They led to an increase in tetradecanoic acid, fructose, tagatose, glucaric acid, glycerol-3P, urea and ethanolamine (precursor of phospholipid phosphatidylethanolamine), and a decrease in levels of 2-hydroxybutyric acid, amino acids (glutamine, valine, leucine, isoleucine, asparagine, serine, arginine, lysine, cysteine, methionine, proline, histidine) and TCA intermediates (aspartic, glutamic and citric acids). Finally, 30 metabolites were differentially expressed between Mix150 and control samples (22 metabolites downregulated and 8 metabolites upregulated, Fig.5A). In particular, we monitored a higher level of octanoic acid (fatty acid), carbohydrates (fructose, tagatose, glucose), urea, and glucaric, glyceric and benzoic acids. Meanwhile, 2-hydroxybutyric acid, myo-inositol, amino acids (A-alanine, lysine, valine, leucine, isoleucine, asparagine, serine, arginine, ornithine, glycine, phenylalanine, cysteine, methionine, proline and threonine) and TCA intermediates (glutamic, lactic and citric acids)

were significantly decreased. The heatmap of modulated metabolites (with *P* value) is provided in Fig.5C (full statistical analysis in supplementary file 11).

To explore the common and specific metabolomic biomarkers, we performed Venn's diagram. As shown in Fig.5B, 7, 5, 11 and 3 metabolites were common to DDT150/PMT150/Mix150, DDT150/Mix150, PMT150/Mix150 and DDT150/PMT150, respectively. The specific modulated metabolites were of 9, 3 and 7 DDT150, PMT150 and Mix150, respectively. Then, we plotted the heatmap of metabolites considering the basal culture medium, biochip controls and the three pesticide treatments (DDT150, PMT150 and Mix150, Fig.S7). The three treatments presented a common signature including the production of lipids (palmitic, decanoic and tetradecanoic acids, and glycerol-3P) and carbohydrates (fructose, tagatose, glucose, sorbitol and glucaric acid). In parallel, we measured low levels of citric acid, aspartic acid, mannose and 2-hydroxybutyric acid. The common metabolites highlighted by Mix150 and PMT150 treatment included low level of glutamine, glutamic acid, leucine, isoleucine, methionine, asparagine, serine, lysine, proline, valine and high level of urea when compared to control and basal medium. Finally, High level of octanoic, benzoic and glyceric acids appeared as specific Mix150 and DDT150 joint markers.

3.4. Transcriptomic and metabolomic integration

In order to gain insights into the action of pesticides, we integrated the metabolomic and transcriptomic data using MetaboAnalyst. The integrated pathway analysis highlighted the central carbon metabolism in cancer pathway in the three treatments (11-26 hits, Fig.6 and supplementary file 12). The DDT150 exposure led to modulation of glycine, serine and threonine metabolism (9 hits), fatty acid biosynthesis (6 hits), PPAR signaling pathway (6 hits), fatty acid degradation (5 hits), necroptosis (9 hits) and insulin resistance (7 hits). Among the pathways perturbated by PMT150 treatment, we extracted the aminoacyl-tRNA biosynthesis, arginine biosynthesis, insulin signaling pathway, insulin resistance, glycerolipid metabolism and fatty acid degradation (15, 8, 8, 7, 5 and 4 hits, respectively). Finally, the analysis with Mix150 DEGs and metabolites returned the following top modulated pathways: insulin signaling pathway (20 hits), PPAR signaling pathway (16 hits), Glucagon signaling pathway (22 hits), MAPK signaling pathway (35 hits) and glutathione metabolism (13 hits).

4. Discussion

In this study, we have investigated the effect of two pesticides (DDT and permethrin: PMT) and their mixtures on rat liver-on-chip. The organ-on-chip technology allows the culture of rat hepatocytes in a controlled micro-environment mimicking physiological conditions. In an attempt to elucidate the mode of action of pesticides, the experiments were coupled to omics profiling. The transcriptomic and metabolomic analysis showed that hepatocytes treated with low-doses of pesticides (15 µM) presented omics profiles similar to control. Contrary, high doses induce major changes in transcriptomic and metabolomic profiles. The analysis of the data contributed to extract a common signature and specific patterns of the tested conditions.

4.1. Common signature of the DDT, PMT and DDT-PMT mixtures

The common signature was illustrated at the transcriptome level by the liver steatosis profile extracted from the toxicity analysis of IPA. This was characterized by the upregulation of the genes *Cyp4a11*, *Ehhadh*, *Hadh, Asah2*, downregulation of *Fabp5*, *Cyp17a1*, *Acaca*, *Tkfc*, and *Lpin1* involved in PPAR signaling, fatty acid and lipid metabolism, and steroid biosynthesis. IPA extracted important lipid transcription factors as potential upstream regulator such as *Srebf1*. Furthermore, the ISMARA processing highlighted the reduction of the motif activity of important liver transcription factors such as HNF4A in the cultures exposed to the pesticides. At the metabolome level, we observed an over expression of various fatty acids and lipids in treated cultures such as the production of decanoic, tetradecanoic and palmitic acids (heatmap of Figs. 5C and S7). The common signature detected in the metabolome included higher level of glucose, fructose and tagatose. Interestingly, high level of fructose is a pro lipogenesis molecule and contribute to steatosis (Hannou et al., 2018). Excess of fructose and glucose can be produced by several sources including the glycogen degradation (we found downregulation of *Gsy2* and *Gbe1*, glycogen storage, in transcriptome data), the tentative of degradation of accumulated lipid (up regulation of *Ehhadh*, *Hadh* involved in fatty acid beta oxydation), the metabolism of glycerol (high level of glycero-3P, activation of the pentose phosphate pathway illustrated by sorbitol and tagatose productions). In parallel, high level of sorbitol is related to degradation of glucose and production of fructose during hyperglycemia (Brownlee 2005). It was correlated in the literature to the reduction of GSH and the increase ROS production (due to the competition of the use of NADPH necessary to produce both the GSH and the aldose reductase required for glucose metabolism into sorbitol). This ROS

increase led to increase the protein kinase C pathway, TGB and NFKB activation and hexoamine over expression (Brownlee 2005). That appeared particularly consistent with the observations in DDT and MIX conditions in which pro inflammatory and necrotic pathways were over activated (see discussion below) when compared to control and PMT cases.

The common mechanism of toxicity also involved a reduction of the CYP450 liver detoxification capability, as far as we detected the downregulation of *Cyp3a5/7* mRNA in all treatment. However, glucuronidation process seems over activated as we detected for all treatment the high level of glucaric acid, a biomarker of this process (Notten et al., 1975). We observed low level of cysteine, an important GSH precursor. Under cysteine limitation, 2-Hydroxybutyric acid is produced as a byproduct of cystathionine conversion to cysteine prior its incorporation into GSH. However, 2-hydroxybutyric acid was downregulated in our dataset. 2-Hydroxybutyric acid is reported to be a liver steatosis biomarker and its production is reported to be an early marker for both insulin resistance and impaired glucose regulation in human (Gall et al., 2010). This difference with the present steatosis like signature illustrated a difference in the pesticides-induced steatosis, when compared to typical metabolic syndrome pathology. In parallel, GST mRNA levels (*Gstt2*, *Gstt2b*, *Mgst2*) were decreased with pesticides treatments. Those enzymes inhibitions impairing the hepatic metabolism is largely reported in pesticide exposure (Ozaslan et al., 2018, Khan et al, 2005). Consistently, our finding illustrated also a weaker capability to detoxify the pesticides *via* the GSH routes and the necessity of an alternative pathway.

The production of α-ketoglutaric acid would illustrate an alternative detoxification pathway. It is report that α-ketoglutaric acid could prevent the lipid peroxidation by increasing enzymatic activity of superoxide dismutase, glutathione peroxidase and catalase to facilitate fat metabolism, and then reduced hepatoxicity in rats (Velvizhi et al., 2002a, 2002b). Nevertheless, we did not find *Sod*, *Gpx* and *Cat* genes upregulation (as those enzymes are also inhibited by some pesticides exposure Khan et al., 2005). Interestingly, tagatose is reported to be an antioxidant and cytoprotective compound, reducing lipid peroxidation in mice hepatocytes presenting GSH depletion under organophosphate exposure (Paterna et al., 1998). It is also an intermediate to D-fructose-6P in the galactose pathway (*Galk*1 gene downregulated). Both fructose and tagatose reduced the iron-dependent reactive oxygen species (ROS)-mediated peroxidation, especially in lipid ROS (Dixon et al., 2012; Dixon and Stockwell 2014). This finding would be particularly consistent in DTT/PMT mixture exposure, in which (i) we

observed that *Ncoa4* and *Sat2* mRNA gene of the iron mediated ROS pathway were modulated (upregulation of *Ncoa4*, downregulation of *Sat2*); (ii) ISMARA highlighted the response to iron (*via Sp1*) and iron chelate transport (*via Maz*).

4.2. DDT specific signature

DDT is reported to conduct to insulin resistance (glucose intolerance and hyperinsulinemia, La Merill et al., 2014). This was consistent with the TF targets of ISMARA that were more particularly linked to insulin response (*via Pml*, *Tfdp1* motifs) and diabetes (*Max* motif). NAFLD with insulin resistance induced by high fat diet and streptozocin are characterized in rat, in addition to typical steatosis response and inflammation (*Tnf*, *p53*, *Nfkb*, by AMPK signaling and the response to insulin, Liu et al., 2017b), which appeared in accord with our finding. Here, the DDT signature is also characterized in the metabolome by high level of arginine, proline and putrescine, and low level of urea and ornithine. At the gene level, is was concomitant with downregulation of *Pycrl* and *Pycr1* (arginine-proline pathway). This suggests a switch from urea production toward putrescine production via the agmatine-putrescine route. First, NAFLD is reported to impair the urea cycle leading to low urea production and high ammonia accumulation in mice (de Chiara et al., 2018). The low ornithine level may also reflect another type of response to the steatosis like behavior. In NAFLD, ornithine is supposed to restore GSH production and alpha ketoglutaric acid reserves to detoxify $NH4^+$ to glutamine (Canbay and Sowa 2019). Secondly, the increase of putrescine in liver is reported to act as protective effect and as a signal for liver regeneration process (Nishiguchi et al., 1990). This result agrees with the modulation at the transcriptome level of *Jak*/*Stat* and interferon signaling (upregulation of *Ifngr1*, *Stat2*, *Ifnar1*) and with literature observation on liver regeneration process in rat (Chen et al., 2010).

Furthermore, ethanolamine appeared strongly increased in the DDT signature (fold change of 11, although P value was of 0.06). It is, with choline, a precursor of phospholipids and promotes rat hepatocyte proliferation and DNA synthesis *via* EGF receptor (Gibellini and Smith 2010; Sasaki et al., 1997; Kume and Sasaki 2006). That is consistent with our observation *Egfr*, *Jat/Stat*, *Met* targets in PML and *Meis3* TFs in ISMARA). Thus, putrescine production may appear as a response of the "de-differentiation like process" (illustrated by the lower transcription factor activity of important liver marker such as *Hnf4a*, *Hnf4g* and *Ahr* extracted by ISMARA) to promote liver regeneration. Finally, the DDT signature also include an over

representation of the gene involved in the cell death, necrosis and inflammation, illustrating a higher toxicity of the compound.

4.3. PMT specific signature

The necrosis and pro-inflammatory pathways were weakly activated at the transcriptome levels when compared to DDT and Mix (PMT/DDT) conditions. PMT is reported to potentiate insulin resistance and to induce steatosis like toxicity (Xiao et al., 2017). Our PMT data were consistent with those finding, but DDT and Mix appeared stronger inducer (see P value and fold change in supplementary file). PMT targeted the mRNA of genes related to ribosomal proteins and to the RNA transport. PMT led to high consumption of TCA substrate (aspartic, glutamic and citric acids), coupled with high consumption of amino acids such as alanine, glutamine (2 oxoglutarate and oxaloacetate entry points), leucine, isoleucine, valine (required for Acetyl-coA and succinyl-CoA productions), asparagine and arginine (fumarate entry point). We observed an opposite profile in PMT and DDT regarding nitrogen metabolism. It is illustrated by the high production of urea in PMT, (whereas we detected high level of allantoin, ornithine in DDT), and the low level of arginine, putrescine, glutamine and glutamic acid in PMT (whereas we found high level of putrescine, arginine in DDT). This set of metabolites would suggest firstly an acid uric metabolism as one potential source of urea production in PMT (allantoin being degraded to urea). Uric acid is a potent antioxidant and interacts with reactive oxygen species (ROS) to be non-enzymatically converted to allantoin (Mikami and Sorimachi 2017). (*nb1*: Uric acid synthesis and transports are also among the targets of two of the top 10 TFs, *Wrnip1_Mta3_Rcor1* and of *Tgif1_Meis3*, in ISMARA PMT and DDT_PMT analysis, but with a lower likelihood when compared to the top 10 targets of the lists reported in supp. file; *nb2* urate processes are not involved in the top 10 TFs related to DDT). This is also consistent with a potential purine metabolism, leading to uric acid as a degradation product of hypoxanthine and guanine (*nb*: both are important component in DNA and RNA, RNA process being particularly highlighted in the PMT exposures). Urea synthesis is impaired in NAFLD (De Chiara et al., 2018), and thus the higher accumulation of urea (when compared to DDT and control) may reflect a moderate steatosis like behavior in PMT cultures (that is consistent with lower level of lipids production when compared to DTT and the PMT/DTT mixture). Finally, the inflammation, cell death messages from the transcriptome analysis appeared weaker in PMT150, suggesting a moderate toxic response when compared to DDT and DDT-PMT mixture.

4.4. Specific mixture signatures

In addition to the steatosis like signature, common to all conditions, the mixture presented a complex signature. A large transcriptome modulation was extracted in which we found the synergy of both pesticides such as the PMT perturbation of the RNA transport, and the DDT perturbation illustrated by the necrotic and inflammation profiles. Furthermore, the signature of those perturbations was enhanced when compared to pure DDT and pure PMT (for instance 14 genes in the RNA transport in mixture vs PMT150, 15 genes in the necroptosis in mixture vs in DDT150). Furthermore, at the metabolome level, we observed the intense depletion of all the amino acids, excepted for cysteine and histidine. We checked if the intense signature of MIX contributed to reproduce a move from NAFLD to NASH. NASH compared to NAFLD is characterized at the metabolome level by accumulation of S-Adenosyl-L-methionine (SAM) and by decreased of *Mat1a* expression in mice (Gitto et al., 2018). We did not observe such tendency for *Mat1a* that was commonly upregulated in Mix150 and PMT150 experiences. SAM synthesis appeared commonly as one target among the top 10 TFs motif of PMT150 and Mix150 analysis in ISMARA (not in DDT).

When compared to literature, the Mix150 signature seemed consistent with the modulation of the immune and inflammatory response, programmed cell death and NF-κB signaling pathway, coupled with low level of methionine, tyrosine, phenylalanine and arginine that is reported in NASH model induced by methionine-choline deficient diet rats (Liu et al., 2017b). Finally, it is reported that the several stage of the NALD (NAFLD, NAFLD with insulin resistance, NASH) depend on the level of chemokine expression, coupled with development of the inflammation, the response *via Nfkb* and with the downstream p53 signalling activation (Liu et al., 2017). This appeared fully consistent with our dataset for Mix 150 treatment.

Conclusion

In summary, we investigated the effects at the transcriptomic and metabolomic level of PMT and DDT, or both together on primary rat hepatocytes cultivated in microfluidic biochips. The pesticides treatments at low-dose (15 µM) presented transcriptome and metabolome profile similar to control. However, multivariate statistical analysis showed a slight separation between low-dose and control groups and complete separation of both from high-dose group, suggesting a dose-dependent effect. At high-dose, the common signature of the three treatments reflected

liver steatosis profile highlighted by the modulation of genes related to PPAR signaling, fatty acid, lipid metabolism and steroid biosynthesis. This profile was confirmed by metabolomic, which showed high level of fatty acids and lipids (decanoic, tetradecanoic and palmitic acids), glucose, fructose and tagatose. As expected, the mixture of DDT and PMT presented a complex signature, with 1349 modulated genes. The Mix150 treatment was characterized by the additive effects of DDT and PMT such as the perturbation of the RNA transport and necrotic/ inflammation profiles specific to PMT and DDT, respectively. Furthermore, these signatures were enhanced, when compared to pure DDT and pure PMT. These results provide an attractive insight into the combination of organ-on-chip and multi-omics to elucidate toxicological effects of pesticides.

Acknowledgement

Conflict of interest

The authors did not report any conflict of interest.

References

Aggerbeck, M., Blanc, E.B., 2018. Role of mixtures of organic pollutants in the development of metabolic disorders via the activation of xenosensors. Curr. Opin. Toxicol. 8, 57-65. http://doi.org/10.1016/j.cotox.2018.01.001.

Al-Eryani, L., Wahlang, B., Falkner, K.C., Guardiola, J.J., Clair, H.B., Prough, R.A., Cave, M., 2015. Identification of environmental chemicals associated with the development of toxicant-associated fatty liver disease in rodents. Toxicol. Pathol. 43, 482-497. https://doi.org/10.1177/0192623314549960.

Balwierz, P.J., Pachkov, M., Arnold, P., Gruber, A.J., Zavolan, M., van Nimwegen, E., 2014. ISMARA: automated modeling of genomic signals as a democracy of regulatory motifs. Genome res. 24, 869-884. https://doi.org/10.1101/gr.169508.113.

Baudoin, R., Alberto, G., Paullier, P., Legallais, C., Leclerc, E., 2012. Parallelized microfluidic biochips in multi well plate applied to liver tissue engineering. Sens. Actuators B Chem. 173, 919-926. https://doi.org/10.1016/j.snb.2012.06.050.

Béranger, R., Hardy, E. M., Dexet, C., Guldner, L., Zaros, C., Nougadère, A., Metten, M. A., Chevrier, C., & Appenzeller, B. (2018). Multiple pesticide analysis in hair samples of pregnant French women: Results from the ELFE national birth cohort. Environ. int. 120, 43–53. https://doi.org/10.1016/j.envint.2018.07.023.

Bervoets, L., Massa, G., Guedens, W., Louis, E., Noben, J.P., Adriaensens, P., 2017. Metabolic profiling of type 1 diabetes mellitus in children and adolescents: a case–control study. Diabetol Metab Syndr. 9, 48. https://doi.org/10.1186/s13098-017-0246-9.

Bricks, T., Paullier, P., Legendre, A., Fleury, M.J., Zeller, P., Merlier, F., Anton, P.M., Leclerc, E., 2014. Development of a new microfluidic platform integrating co-cultures of intestinal and liver cell lines. Toxicol. in Vitro. 28, 885-895. https://doi.org/10.1016/j.tiv.2014.02.005.

Brockmeier, E.K, Hodges, G., Hutchinson, T.H., Butler, E., Hecker, M., Tollefsen, K.E., Garcia-Reyero, N., Kille, P., Becker, D., Chipman, K., Colbourne, J., Collette, T.W., Cossins, A., Cronin, M., Graystock, P., Gutsell, S., Knapen, D., Katsiadaki, I., Lange, A., Marshall, S., Owen, S.F., Perkins, E.J., Plaistow, S., Schroeder, A., Taylor, D., Viant, M., Ankley, G., Falciani, F., 2017. The role of omics in the application of adverse outcome pathways for chemical risk assessment. Toxicol. Sci. 158, 252-262. https://doi.org/10.1093/toxsci/kfx097.

Brownlee, M., 2005. The pathobiology of diabetic complications: a unifying mechanism. Diabetes 54, 1615-1625. https://doi.org/10.2337/diabetes.54.6.1615.

Canbay, A., Sowa, J.P., 2019. L-Ornithine L-Aspartate (LOLA) as a novel approach for therapy of non-alcoholic fatty liver disease. Drugs, 39-44. https://doi.org/10.1007/s40265-018-1020-5.

Canzler, S., Schor, J., Busch, W., Schubert, K., Rolle-Kampczyk, U.E., Seitz, H., Kamp, H., von Bergen, M., Buesen, R., Hackermüller, J., 2020. Prospects and challenges of multi-omics data integration in toxicology. Arch. Toxicol. 94, 371-388. https://doi.org/10.1007/s00204-020-02656-y.

Chen, X., Xu, C., Zhang, F., Ma, J., 2010. Microarray approach reveals the relevance of interferon signaling pathways with rat liver restoration post 2/3 hepatectomy at cellular level. J. interferon cytokine res. 30, 525-539. https://doi.org/10.1089/jir.2009.0111.

Chong, J., Soufan, O., Li, C., Caraus, I., Li, S., Bourque, G., Wishart, D.S, Xia, J., 2018. MetaboAnalyst 4.0: towards more transparent and integrative metabolomics analysis. Nucl. Acids Res. 46, W486-494. https://doi.org/10.1093/nar/gky310.

Choucha- Snouber, L., Aninat, C., Grsicom, L., Madalinski, G., Brochot, C., Poleni, P.E., Razan, F., Guguen Guillouzo, C., Legallais, C., Corlu, A., Leclerc, E., 2013. Investigation of ifosfamide nephrotoxicity induced in a liver–kidney co- culture biochip. Biotechnol. Bioeng. 110, 597-608. https://doi.org/10.1002/bit.24707.

Choucha Snouber, L., Jacques, S., Monge, M., Legallais, C., Leclerc, E., 2012. Transcriptomic analysis of the effect of ifosfamide on MDCK cells cultivated in microfluidic biochips. Genomics 100, 27-34. https://doi.org/10.1016/j.ygeno.2012.05.001.

De Abrew, K.N., Overmann, G.J., Adams, R.L., Tiesman, J.P., Dunavent, J., Shan, Y. K., Carr, G.J., Daston, G.P., Naciff, J.M., 2015. A novel transcriptomics based in vitro method to compare and predict hepatotoxicity based on mode of action. Toxicology 328, 29-39. https://doi.org/10.1016/j.tox.2014.11.008.

De Chiara, F., Heebøll, S., Marrone, G., Montoliu, C., Hamilton-Dutoit, S., Ferrandez, A., Andreola, F., Rombouts, K., Grønbæk, H., Felipo, V., Gracia-Sancho, J., Mookerjee, R.P., Vilstrup, H., Jalan, R., Thomsen, K.L., 2018. Urea cycle dysregulation in non-alcoholic fatty liver disease. J. hepatol. 69, 905-915. https://doi.org/10.1016/j.jhep.2018.06.023.

Dixon, S.J., Lemberg, K.M., Lamprecht, M.R., Skouta, R., Zaitsev, E.M., Gleason, C.E., Patel, D.N., Bauer, A.J., Cantley, A.M., Yang, W.S., Morrison, B., Stockwell, B.R., 2012. Ferroptosis: an iron-dependent form of nonapoptotic cell death. Cell 149, 1060-1072. https://doi.org/10.1016/j.cell.2012.03.042.

Dixon, S.J., Stockwell, B.R., 2014. The role of iron and reactive oxygen species in cell death. Nat. Chem. Biol. 10, 9-17. https://doi.org/10.1038/nchembio.1416.

Essaouiba, A., Okitsu, T., Kinoshita, R., Jellali, R., Shinohara, M., Danoy, M., Legallais, C., Sakai, Y., Leclerc, E., 2020b. Development of a pancreas-liver organ-on-chip coculture model for organ-to-organ interaction studies. Biochem. Eng. J. 164, 107783. https://doi.org/10.1016/j.bej.2020.107783.

Fedeli, D., Montani, M., Bordoni, L., Galeazzi, R., Nasuti, C., Correia-Sá, L., Domingues, V. F., Jayant, M., Brahmachari, V., Massaccesi, L., Laudadio, E., & Gabbianelli, R. (2017). In vivo and in silico studies to identify mechanisms associated with Nurr1 modulation following early life exposure to permethrin in rats. Neuroscience, 340, 411-423. https://doi.org/10.1016/j.neuroscience.2016.10.071.

Fiehn, O., 2006. Metabolite profiling in Arabidopsis. Methods Mol. Biol. 323, 439-447. https://doi.org/10.1385/1-59745-003-0:439.

Fiehn, O., Wohlgemuth, G., Scholz, M., Kind, T., Lee, D.Y., Lu, Y., Moon, S., Nikolau, B., 2008. Quality control for plant metabolomics: reporting MSI-compliant studies. Plant J. 53, 691-704. https://doi.org/10.1111/j.1365-313X.2007.03387.x.

Gall, W.E., Beebe, K., Lawton, K.A., Adam, K.P., Mitchell, M.W., Nakhle, P.J., Ryals, J.A., Milburn, M.V., Nannipieri, M., Camastra, S., Natali, A., Ferrannini, E., RISC Study Group., 2010. alpha-hydroxybutyrate is an early biomarker of insulin resistance and glucose intolerance in a nondiabetic population. PloS one 5, e10883. https://doi.org/10.1371/journal.pone.0010883.

Ghisari, M., Long, M., Tabbo, A., Bonefeld-Jørgensen, E.C., 2015. Effects of currently used pesticides and their mixtures on the function of thyroid hormone and aryl hydrocarbon receptor in cell culture. Toxicol. Appl. Pharmacol. 284, 292-303. https://doi.org/10.1016/j.taap.2015.02.004.

Gibellini, F., Smith, T.K., 2010. The Kennedy pathway--De novo synthesis of phosphatidylethanolamine and phosphatidylcholine. IUBMB life 62, 414-428. https://doi.org/10.1002/iub.337.

Gitto, S., Schepis, F., Andreone, P., Villa, E., 2018. Study of the serum metabolomic profile in nonalcoholic fatty liver disease: Research and clinical perspectives. Metabolites 8, 17. https://doi.org/10.3390/metabo8010017.

Hannou, S.A., Haslam, D.E., McKeown, N.M., Herman, M.A., 2018. Fructose metabolism and metabolic disease. J. Clin. Invest. 128, 545-555. https://doi.org/10.1172/JCI96702.

Harada, T., Takeda, M., Kojima, S., Tomiyama, N., 2016. Toxicity and carcinogenicity of dichlorodiphenyltrichloroethane (DDT). Toxicol. Res. 32, 21-33. https://doi.org/10.5487/TR.2016.32.1.021.

He, B., Ni, Y., Jin, Y., Fu, Z., 2020. Pesticides-induced energy metabolic disorders. Sci. Total Environ. 729, 139033. https://doi.org/10.1016/j.scitotenv.2020.139033.

Howell, G.E., Mulligan, C., Meek, E., Chambers, J.E., 2015. Effect of chronic p,p'-dichlorodiphenyldichloroethylene (DDE) exposure on high fat diet-induced alterations in glucose and lipid metabolism in male C57BL/6H mice. Toxicology 328, 112-122. https://doi.org/10.1016/j.tox.2014.12.017.

Hu, X., Li, S., Cirillo, P., Krigbaum, N., Tran, V., Ishikawa, T., La Merrill, M.A., Jones, D.P., Cohn, B., 2020. Metabolome Wide Association Study of serum DDT and DDE in

Pregnancy and Early Postpartum. Reprod. Toxicol. 92, 129-137. https://doi.org/10.1016/j.reprotox.2019.05.059.

Huq, F., Obida, M., Bornman, R., Lenardo, T.Z., Chevrier, J., 2020. Associations between prenatal exposure to DDT and DDE and allergy symptoms and diagnoses in the Venda Health Examination of Mothers, Babies and their Environment (VHEMBE), South Africa. Environ. Res. 185, 109366. https://doi.org/10.1016/j.envres.2020.109366.

Jeffries, K.M., Komoroske, L.M., Truong, J., Werner, I., Hasenbein, M., Hasenbein, S., Fangue, N.A., Connon, R.E., 2015. The transcriptome-wide effects of exposure to a pyrethroid pesticide on the Critically Endangered delta smelt Hypomesus transpacificus. Endang. Species Res. 28, 43-60. https://doi.org/10.3354/esr00679.

Jellali, R., Bricks, T., Jacques, S., Fleury, M.J., Paullier, P., Merlier, F., Leclerc, E., 2016a. Long- term human primary hepatocyte cultures in a microfluidic liver biochip show maintenance of mRNA levels and higher drug metabolism compared with Petri cultures. Biopharm. drug dispos. 37, 264-275. https://doi.org/10.1002/bdd.2010.

Jellali, R., Paullier, P., Fleury, M. J., Leclerc, E., 2016. Liver and kidney cells cultures in a new perfluoropolyether biochip. Sens. Actuators B Chem. 229, 396-407. https://doi.org/10.1016/j.snb.2016.01.141.

Jellali, R., Gilard, F., Pandolfi, V., Legendre, A., Fleury, M.J., Paullier, P., Legallais, C., Leclerc, E., 2018a. Metabolomics-on-a-chip approach to study hepatotoxicity of DDT, permethrin and their mixtures. J. Appl. Toxicol. 38, 1121-1134. https://doi.org/10.1002/jat.3624.

Jellali, R., Zeller, P., Gilard, F., Legendre, A., Fleury, M.J., Jacques, S., Tcherkez, G., Leclerc, E., 2018. Effects of DDT and permethrin on rat hepatocytes cultivated in microfluidic biochips: Metabolomics and gene expression study. Environ. Toxicol. Pharmacol. 59, 1-12. https://doi.org/10.1016/j.etap.2018.02.004.Jin, X., Chen, M., Song, L., Li, H., Li, Z., 2014. The evaluation of p,p'-DDT exposure on cell adhesion of hepatocellular carcinoma. Toxicology. 322, 99-108. https://doi.org/10.1016/j.tox.2014.05.002.

Joseph P., 2017. Transcriptomics in toxicology. Food chem. Toxicol. 109, 650-662. https://doi.org/10.1016/j.fct.2017.07.031.

Khan, S.M., Sobti, R.C., Kataria, L., 2005. Pesticide-induced alteration in mice hepato-oxidative status and protective effects of black tea extract. Clin. Chim. acta 358, 131-138. https://doi.org/10.1016/j.cccn.2005.02.015.

Kimura, H., Sakai, Y., Fujii, T., 2018. Organ/body-on-a-chip based on microfluidic technology for drug discovery. Drug Metab. Pharmacokinet. 33, 43-48. https://doi.org/10.1016/j.dmpk.2017.11.003.

Kostka, G., Palut, D., Kopeć-Szlezak, J., Ludwicki, J. K., 2000. Early hepatic changes in rats induced by permethrin in comparison with DDT. Toxicology 142, 135-143. https://doi.org/10.1016/s0300-483x(99)00164-x.

Krauskopf, J., de Kok, T.M., Hebels, D.G., Bergdahl, I.A., Johansson, A., Spaeth, F., Kiviranta, H., Rantakokko, P., Kyrtopoulos, S.A., Kleinjans, J. C., 2017. MicroRNA profile for health risk assessment: Environmental exposure to persistent organic pollutants strongly affects the human blood microRNA machinery. Sci. rep. 7, 9262. https://doi.org/10.1038/s41598-017-10167-7.

Kume, H., Sasaki, H., 2006. Ethanolamine modulates DNA synthesis through epidermal growth factor receptor in rat primary hepatocytes. In Vitro cell. Dev. Biol. Anim. 42, 20-26. https://doi.org/10.1007/s11626-006-0007-9.

Leibold, E., Schwarz, L.R., 1993. Inhibition of intercellular communication in rat hepatocytes by phenobarbital, 1,1,1-trichloro-2,2-bis(p-chlorophenyl)ethane (DDT) and gamma-hexachlorocyclohexane (lindane): modification by antioxidants and inhibitors of cyclo-oxygenase. Carcinogenesis 14, 2377-2382. https://doi.org/10.1093/carcin/14.11.2377.

La Merrill, M., Karey, E., Moshier, E., Lindtner, C., La Frano, M.R., Newman, J.W., Buettner, C., 2014. Perinatal exposure of mice to the pesticide DDT impairs energy expenditure and metabolism in adult female offspring. PloS one 9, e103337. https://doi.org/10.1371.

Liang, Y.J., Wang, H.P., Long, D.X., Li, W., Wu, Y.J., 2013. A metabonomic investigation of the effects of 60 days exposure of rats to two types of pyrethroid insecticides. Chem. Biol. Interact. 206, 302-308. https://doi.org/10.1016/j.cbi.2013.10.002.

Liu, X.L., Ming, Y.N., Zhang, J.Y., Chen, X.Y., Zeng, M.D., Mao, Y.M., 2017b. Gene-metabolite network analysis in different nonalcoholic fatty liver disease phenotypes. Exp. Mol. Med. 49, e283. https://doi.org/10.1038/emm.2016.123.

Liu, Q., Wang, Q., Xu, C., Shao, W., Zhang, C., Liu, H., Jiang, Z., Gu, A., 2017a. Organochloride pesticides impaired mitochondrial function in hepatocytes and aggravated disorders of fatty acid metabolism. Sci. rep. 7, 46339. https://doi.org/10.1038/srep46339.

Merlier, F., Jellali, R., Leclerc, E., 2017. Online hepatic rat metabolism by coupling liver biochip and mass spectrometry. Analyst 142, 3747-3757. https://doi.org/10.1039/C7AN00973A.

Mikami, T., Sorimachi, M., 2017. Uric acid contributes greatly to hepatic antioxidant capacity besides protein. Physiol. Res. 66, 1001-1007. https://doi.org/10.33549/physiolres.933555.

Morales-Prieto, N., Ruiz-Laguna, J., Sheehan, D., Abril, N., 2018. Transcriptome signatures of p,p′-DDE-induced liver damage in Mus spretus mice. Environ. Pollut. 238, 150-167. https://doi.org/10.1016/j.envpol.2018.03.005.

Nishiguchi, S., Kuroki, T., Takeda, T., Nakajima, S., Shiomi, S., Seki, S., Matsui-Yuasa, I., Otani, S., Kobayashi, K., 1990. Effects of putrescine on D-galactosamine-induced acute liver failure in rats. Hepatology 12, 348-353. https://doi.org/10.1002/hep.1840120224.

Notten, W.R.F., Henderson, P.T., Kuyper, C.M.A., 1975. Stimulation of the glucuronic acid pathway in isolated rat liver cells by phenobarbital. Internation. J. Biochem. 6, 713-718.

Özaslan, M.S., Demir, Y., Aksoy, M., Küfrevioğlu, Ö.I., Beydemir, Ş., 2018. Inhibition effects of pesticides on glutathione-S-transferase enzyme activity of Van Lake fish liver. J. Biochem. Mol. Toxicol. 32, e22196. https://doi.org/10.1002/jbt.22196.

Paterna, J.C., Boess, F., Stäubli, A., Boelsterli, U.A., 1998. Antioxidant and cytoprotective properties of D-tagatose in cultured murine hepatocytes. Toxicol. Appl. Pharmacol. 148, 117-125. https://doi.org/10.1006/taap.1997.8315.

Peng, S., Kong, D., Li, L., Zou, C., Chen, F., Li, M., Cao, T., Yu, C., Song, J., Jia, W., Peng, P., 2020. Distribution and sources of DDT and its metabolites in porewater and sediment from a typical tropical bay in the South China Sea. Environ. Pollut. 267, 115492. https://doi.org/10.1016/j.envpol.2020.115492.

Prot, J.M., Bunescu, A., Elena-Herrmann, B., Aninat, C., Snouber, L.C., Griscom, L., Razan, F., Bois, F.Y., Legallais, C., Brochot, C., Corlu, A., Dumas, M.E., Leclerc, E., 2012. Predictive toxicology using systemic biology and liver microfluidic "on chip" approaches: application to acetaminophen injury. Toxicol. Appl. Pharmacol. 259, 270-280. https://doi.org/10.1016/j.taap.2011.12.017.

Rizzati, V., Briand, O., Guillou, H., Gamet-Payrastre, L., 2016. Effects of pesticide mixtures in human and animal models: An update of the recent literature. Chem. Biol. Interact. 254, 231-246. https://doi.org/10.1016/j.cbi.2016.06.003.

Roede, J.R., Uppal, K., Park, Y., Tran, V., Jones, D.P., 2014. Transcriptome-metabolome wide association study (TMWAS) of maneb and paraquat neurotoxicity reveals network level interactions in toxicologic mechanism. Toxicol. Rep. 1, 435-444. https://doi.org/10.1016/j.toxrep.2014.07.006.

Russo, F., Ceci, A., Pinzari, F., Siciliano, A., Guida, M., Malusà, E., Tartanus, M., Miszczak, A., Maggi, O., Persiani, A.M., 2019. Bioremediation of dichlorodiphenyltrichloroethane

(DDT)-contaminated agricultural soils: potential of two autochthonous saprotrophic fungal strains. Appl. Environ. Microbiol. 85, e01720-19. https://doi.org/10.1128/AEM.01720-19.

Sasaki, H., Kume, H., Nemoto, A., Narisawa, S., Takahashi, N., 1997. Ethanolamine modulates the rate of rat hepatocyte proliferation in vitro and in vivo. Proc. Natl. Acad. Sci. USA 94, 7320-7325. https://doi.org/10.1073/pnas.94.14.7320.

Seglen, P.O., 1976. Preparation of isolated rat liver cells. Methods Cell Biol. 13, 29-83.

Song, N.E., Lee, J.Y., Mansur, A.R., Jang, H.W., Lim, M.C., Lee, Y., Yoo, M., Nam, T.G., 2019. Determination of 60 pesticides in hen eggs using the QuEChERS procedure followed by LC-MS/MS and GC-MS/MS. Food chem. 298, 125050. https://doi.org/10.1016/j.foodchem.2019.125050.

Song, Q., Chen, H., Li, Y., Zhou, H., Han, Q., & Diao, X. (2016). Toxicological effects of benzo(a)pyrene, DDT and their mixture on the green mussel Perna viridis revealed by proteomic and metabolomic approaches. Chemosphere, 144, 214-224. https://doi.org/10.1016/j.chemosphere.2015.08.029.

Štampar, M., Frandsen, H.S., Rogowska-Wrzesinska, A., Wrzesinski, K., Filipič, M., Žegura, B., 2020. Hepatocellular carcinoma (HepG2/C3A) cell-based 3D model for genotoxicity testing of chemicals. Sci. Total Environ. 143255. https://doi.org/10.1016/j.scitotenv.2020.143255.

Velvizhi, S., Dakshayani, K.B., Subramanian, P., 2002a. Effects of alpha-ketoglutarate on antioxidants and lipid peroxidation products in rats treated with ammonium acetate. Nutrition 18, 747-750. https://doi.org/10.1016/s0899-9007(02)00825-0.

Velvizhi, S., Nagalashmi, T., Essa, M.M., Dakshayani, K.B., Subramanian, P., 2002b. Effects of alpha-ketoglutarate on lipid peroxidation and antioxidant status during chronic ethanol administration in Wistar rats. Pol. J. Pharmacol. 54, 231-236.

VoPham, T., Bertrand, K.A., Hart, J.E., Laden, F., Brooks, M.M., Yuan, J.M., Talbott, E.O., Ruddell, D., Chang, C.H., Weissfeld, J.L., 2017. Pesticide exposure and liver cancer: a review. Cancer causes control 28, 177-190. https://doi.org/10.1007/s10552-017-0854-6.

Wang, X., Martínez, M.A., Dai, M., Chen, D., Ares, I., Romero, A., Castellano, V., Martínez, M., Rodríguez, J.L., Martínez-Larrañaga, M.R., Anadón, A., Yuan, Z., 2016. Permethrin-induced oxidative stress and toxicity and metabolism. A review. Environ. Res. 149, 86-104. https://doi.org/10.1016/j.envres.2016.05.003.

Wang, Z., Gerstein, M., Snyder, M., 2009. RNA-Seq: a revolutionary tool for transcriptomics. Nat. rev. Genet. 10, 57-63. https://doi.org/10.1038/nrg2484.

Willemin, M.E., Desmots, S., Le Grand, R., Lestremau, F., Zemana, F.A., Leclerc, E., Moesch, C., Brochot, C., 2016. PBPK modeling of the cis- and trans-permethrin isomers and their major urinary metabolites in rats. Toxicol. Appl. Pharmacol. 294, 65-77. https://doi.org/10.1016/j.taap.2016.01.011.

Willemin, M.E., Kadar, A., de Sousa, G., Leclerc, E., Rahmani, R., Brochot, C., 2015. In vitro human metabolism of permethrin isomers alone or as a mixture and the formation of the major metabolites in cryopreserved primary hepatocytes. Toxicol. in vitro 29, 803-812. https://doi.org/10.1016/j.tiv.2015.03.003

Wu, J.P., Peng, Y., Zhi, H., Chen, X.Y., Wu, S.K., Tao, L., Zeng, Y.H., Luo, X.J., Mai, B.X., 2019. Contamination of organohalogen chemicals and hepatic steatosis in common kingfisher (Alcedo atthis) breeding at a nature reserve near e-waste recycling sites in South China. Sci. Total Environ. 659, 561-567. https://doi.org/10.1016/j.scitotenv.2018.12.395.

Xiang, D., Chu, T., Li, M., Wang, Q., Zhu, G., 2018. Effects of pyrethroid pesticide cis-bifenthrin on lipogenesis in hepatic cell line. Chemosphere. 201, 840-849. https://doi.org/10.1016/j.chemosphere.2018.03.009.

Xiao, X., Kim, Y., Kim, D., Yoon, K.S., Clark, J.M., Park, Y., 2017. Permethrin alters glucose metabolism in conjunction with high fat diet by potentiating insulin resistance and decreases voluntary activities in female C57BL/6J mice. Food Chem. Toxicol. 108, 161-170. https://doi.org/10.1016/j.fct.2017.07.053.

Xiao, X., Sun, Q., Kim, Y., Yang, S.H., Qi, W., Kim, D., Yoon, K.S., Clark, J. M., Park, Y., 2018. Exposure to permethrin promotes high fat diet-induced weight gain and insulin resistance in male C57BL/6J mice. Food Chem. Toxicol. 111, 405-416. https://doi.org/10.1016/j.fct.2017.11.047.

Yang, J.S., Qi, W., Farias-Pereira, R., Choi, S., Clark, J.M., Kim, D., Park, Y., 2019. Permethrin and ivermectin modulate lipid metabolism in steatosis-induced HepG2 hepatocyte. Food Chem. Toxicol. 125, 595-604. https://doi.org/10.1016/j.fct.2019.02.005.

Yang, J. S., Park, Y., 2018. Insecticide exposure and development of nonalcoholic fatty liver disease. J. agric. food chem. 66, 10132-10138. https://doi.org/10.1021/acs.jafc.8b03177.

Zucchini-Pascal, N., Peyre, L., de Sousa, G., Rahmani, R., 2012. Organochlorine pesticides induce epithelial to mesenchymal transition of human primary cultured hepatocytes. Food chem. Toxicol. 50, 3963-3970. https://doi.org/10.1016/j.fct.2012.08.009.

Zuluaga, M., Melchor, J.J., Tabares- Villa, F.A., Taborda, G., Sepulveda- Arias, J.C., 2016. Metabolite profiling to monitor organochlorine pesticide exposure in HepG2 cell culture. Chromatographia 79, 1061-1068. https://doi.org/10.1007/s10337- 016- 3031- 2.

Table 1

Click here to access/download;Table;Table 1.docx ⬇

Table 1. Top ten transcription factors extracted by ISMARA processing comparing DDT and Control,

	Canonical pathway (P value, Hits)	Tox function/ tox list (P value, Hits)	Upstream regulators (P value)
DDT150 vs. CT	Glutathione-mediated detoxification ($3e^{-4}$, 4)	Liver steatosis ($1.13e^{-7}$, 20)	*Ucp1* ($4e^{-9}$)
	LPS/IL-1 mediated inhibition of RXR unction (0.002, 9)	Liver inflammation/hepatitis (0.0003, 14)	*Srebf1* ($4.77e^{-9}$)
	Tryptophan degradation (0.0028, 3)	Liver necrosis/cell death (0.0008, 9)	*Insig1* ($1.1e^{-6}$)
	Proline biosynthesis II (from Arginine) (0.0029, 2)	Glutathione depletion-phase II reactions (0.001, 3)	TO-901317 ($5e^{-6}$)
	Arginine degradation VI (0.0029, 2)	LPS/IL-1 mediated inhibition of RXR function (0.0016, 10)	*Ifnb1* ($7e^{-6}$)
PMT150 vs. CT	Glycogen biosynthesis II (0.0019, 2)	Liver steatosis (0.003, 12)	*Ucp1* ($2.7e^{-7}$)
	LPS/IL-1 mediated inhibition of RXR Function (0.007, 8)	Liver cirrhosis (0.02, 1)	*Rxrg* ($5.4e^{-7}$)
	Fatty acid β-oxidation I (0.009, 3)	CAR/RXR activation (0.004, 3)	*Srebf1* (0.0002)
	Adipogenesis pathway (0.009, 6)	LPS/IL-1 mediated inhibition of RXR function (0.01, 8)	*Ppara* (0.00028)
	IL-17A signaling in fibroblasts (0.01, 3)	Fatty Acid Metabolism (0.01, 5)	*Mlxipl* (0.0003)
Mix150 vs. CT	Fatty Acid β-oxidation III (3.5×10^{-5}, 4)	Liver necrosis/cell death (0.0008, 26)	miR-16-5p ($1.4e^{-11}$)
	MAPK signaling (0.001, 13)	Liver inflammation/hepatitis (0.002, 40)	*Hnf4a* ($1.2e^{-9}$)
	TGF-β signaling (0.002, 15)	Liver steatosis (0.003, 41)	*Ppara* ($1.1e^{-7}$, 14)
	Estrogen receptor signaling (0.003, 18)	Mechanism of gene regulation by peroxisome Proliferators via PPARα ($8.3e^{-4}$, 17)	miR-30c-5p ($1.9e^{-7}$, 14)
	ErbB2-ErbB3 signaling (0.005, 12)	TGF-β signaling ($9.7e^{-4}$, 16)	TO-901317 ($4e^{-7}$, 14)

Table 2

Table 2. Top ten transcription factors extracted by ISMARA processing comparing DDT and Control. [HCP] corresponded to the gene of the Motif name having the strongest (absolute value) coefficient of Pearson; Motif logo is associated to the HCP gene ; Profil correspond to the biochip location with the high activity of the motif ; Potential liver target are extracted from supplementary file 5.

Motif info	Z_value	Potential liver target
MAX_MYCN [MAX] CT GAGCACGTGGT	4,13	*Esra_Esrb*, *Sox8*, *Fasn*, *Fabp5*, *Slc2a5*, *Pdp2* genes Lipid, triglyceride, acetylCoA synthesis process Bile acids, fructose transports, androgen R activity, pyruvate DH complex, glucose transporters, polyamines reactomes
HOXB7 [HOXB7] DDT TAAT	4,07	*Esrg*, *Nr4a1_Nr2f1* genes IFN process, NFKB pathway Apoptotic cleavage reactome
CDH1_PML [PML] DDT CCGCCGCCGC TGCCGCCGC	3,10	*Ppard*, *Hnf6* genes EGFR, JAT/STAT, choline signallings MET, insulin, NFKB, pathways
YY1_YY2 [YY1] CT GCCATC	2,73	Ribosomal process Oxygen transporter, NADH activities Mitonchondrial protein, respiratory electron transport reactomes
NFIA [NFIA] CT CTTGGCA	2,48	*Nr1h4*, *Cyp17a1*, *G6pc*, *Fgf21* genes Iron chelate transport, response to methionine, to acetate, triglyceride biosynthesis, G6PC transport HNF3B, RXR/VDR pathways, programmed cell death Glucuronidation, glucose transport, GSH, androgen reactomes
TFDP1_WT1_EGR2 [TFDP1] DDT GGCGCG	2,46	Lipoprotein lipase activity, insulin/glucose interaction Insulin, IL6, TGFb, IFNg pathways ECM regulators TGFb/EMT, SMADs, cell cycles, insulin secretion reactomes
HEY1_MYC_MXI1 [MIX1] CT CCACGTG	2,36	*Fabp5*, *Srm*, *Ifrd2*, *Prmt1* genes Spermidine, choline synthesis Fructose transport, ribosomal process, Androgen R, G2/M, FAS pathways Pyruvate DH, gluconeogenesis, glucose transport reactomes
TGIF1_MEIS3 [MEIS3] DDT TTGACAGG	2,21	*Foxa2_Foxa1*, *Nr5a2*, *Esrg*, *Pou4f3*, *Acss2*, *Ces2i*, *Ces2a* genes Urea cycle, homocysteine process, GSH process AP1, androgen R, EGFR, HNF3B pathways Fatty acid b oxidation, glycoshingolipid, IFNg reactomes
ATF4 [ATF4] CT GGATGATGCAATA	2,08	*Fgf21*, *Chac1*, *Inhbe* genes Response to methionine, GSH process, serine biosynthesis, lipoprotein process, rrginine transport, TGFb-R, iL1 , FGF-R bindings Amino acid process and transport reactomes
HIC2 [HIC2] CT ATGCCCACC	1,91	*Nr2f1_Nr4a1*, *Fgf6* genes Wnt signaling via JNK, P53 binding P38-MAPK, iL12-STAT4, IFNg, FGF reactomes,

Table 3

Click here to access/download;Table;Table 3.docx ⬇

Table 3. Top ten transcription factors extracted by ISMARA processing comparing PMT and Controls, sorted by z_value. HCP corresponded to the gene of the Motif name having the strongest (absolute value) coefficient of Pearson ; Motif logo is associated to the HCP gene ; Profil correspond to the biochip location with the high activity of the motif ; Potential liver target are extracted from supplementary file 7.

Motif info	Z_value	Potential liver target
MAX_MYCN [MAX] CT GAGCACGTGGT	3,74	*Fasn*, *Slc2a5*, *Pdp2* genes RNA process, IFNb production, Lipid synthesis process Fructose binding, IL1, IGF1, HIF1pathways, p53 effectors Pyruvate DH complex, diabetes pathway reactomes
ZFP110 [ZFP110] CT TAGGGTTTCTCT CCAGTATG	3,03	Response to retinoic acid, glycogen process WNT/Ca2+/GMP signalling
WRNIP1_MTA3_ RCOR1 [MTA3] PMT CCTCCTCCCC	2,80	Hexoses, glucose transports, ECM reactome Ion, amine, carbohydrates, organic acids, bile salts transports reactomes
E2F1 [E2F1] CT CTGGCGGGAA	2,45	*Foxa1_Foxa2* genes E2F, ATM, ERK-MAPK pathways Cell cycle damage reactome, polyamine metabolism reactome
SNAI1_ZEB1_SN AI2 [ZEB1] PMT CTCACCTG	2,33	*Nr2f6*, *Foxl1_Foxo1*, *Foxo6*, *Pou4f3*, *Pou2f3*, *Bmp3* genes Regulation of epidermal cell, energy-proton transport, SMAD traduction process WNT/Ca2+/GMP signaling, NFAT, WNT, FGF, TNF, RXR/VDR pathways NOTCH, amine ligand reactomes
POU1F1 [POU1F1] PMT AATTCATAATTA TATACA	2,31	*Pparg_Rxrg*, *Hnf4a* genes ECM related pathways
HSF2 [HSF2] CT AGAATGTTCT	2,22	*Cyp17a1* RNA DNA process, response to acetate GPX activity, ECM binding Sterol, aquaporins transport, alcohol oxidation reactomes
ZBTB33_CHD2 [CHD2] CT TCTCGCAGATT T	2,22	RNA process, ribosomal binding Iron responsive element binding mTOR pathway, Hippo signaling
TGIF1_MEIS3 [TGIF1] PMT TGACAG	2,19	*Foxa2_Foxa1, Hnf1b*, *Esrg*, *Pou4f3*, *Ces2a* genes Choline, SAM, GSH processes, ECM signaling WNT, RXR/VDR, HNF3B pathways ECM, Lipid, GSH, sulfur amino acid metab. reactomes
ETV1_ETV5_GA BPA [GABPA] CT CAATACCGGAA GTGTA	2,09	RNA, ribosomal process, mitochondrial signal cMYC, cell cycle, HIF1 pathway p53 reactome, RNA related reactome

Table 4

Table 4. Top ten transcription factors extracted by ISMARA processing comparing MIX and Controls, sorted by z_value. HCP corresponded to the gene of the Motif name having the strongest (absolute value) coefficient of Pearson ; Motif logo is associated to the HCP gene ; Profil correspond to the biochip location with the high activity of the motif ; Potential liver target are extracted from Supplementary file 9.

Motif info	Z_value	Potential liver target
CHD1_PML [CHD1] MIX CGCCGCCGCCC CCGC	7,48	*Ppard*, *Foxo6*, *Mycbp2*, *Chd2* genes JAK/STAT signaling, HNF3A, MET, b Catenin, NFKB pathways Adherent junctions reactome
ZFX_ZFP711 [ZFX] MIX GGGGGCCCCAG GCCTCGGC	5,84	*Ppard*, *Foxo6* genes Phospholipid translocation TNF, p53, NOTCH, HIF1A, iL5 pathways
MAX_MYCN [MAX] CT GAGCACGTGGT	5,56	*Essra_Essrb*, *Smad2*, *Sox8*, *Fasn*, *Slc2a5*, *Fabp5*, *Prmt1* genes Ribosomal process, fatty acid, triglyceride process fructose transport HIF, ECM, WNT, Androgen-R pathways
MECP2 [MECP2] MIX CCCGGAG	5,10	*Ahr*, *Foxo3*, *Foxo6*, *Nr4a2*, *Nox4* genes Protein palmitoylation, homocysteine process TNF, EGF, TGFb, ECM, WNT, Androgen-R pathways Sphingolipid synthesis, insulin secretion reactome
MAZ_ZFP281 [MAZ] CT GGGGGGGGGAG GGAGGG	4,19	Fatty acid synthesis, iron chelate transport HIF, ECM, MYC pathways Collagen, Glycolysis, glucagon, IGF reactomes
NRF1 [NRF1] MIX TGCGCATGCGCA GTG	4,15	*Pou2f1*, *Foxo3*, *Smad4*, *Onecut1_Cux2* genes iL1, ERK/MAPK, BMP, JNK/MAPK, androgen-R pathways ABCA transporters in lipid homeostasis, Insulin process, respiration electron transport reactomes
IRF2_IRF1_IRF8_IRF9_IRF7 [IRF7] MIX AAGGAAAGCGAA ACCGAAAC	3,86	*Stat1*, *Stat2*, *Cxcl10*, *Cxcl16*, *Cxcl11* genes WNT regulation, SAM synthesis, response to IFNg FOXO signaling, cytokine related pathways Sulfur amino acid metab, Hippo, IFN, chemokines reactome
ATF4 [ATF4] CT GGATGATGCAAT A	3,72	*Cebpa_Cebpg*, *Fgf21*, *Inhbe*, *Chac1* genes Response to methionine, regulation of lipoprotein, GSH, L-serine, arginine processes P38 signalling, AP1, iL4 pathways TGFb, Amino acid synthesis, IFN reactomes
SP1 [SP1] MIX GGGGGCGGGGC	3,54	*Hif*, *Foxo3*, *Ahr*, *Abca5* genes Response to iron NFKB, p38, HNF3B, FAS, lysophospholipid pathways Adherent junctions, ECM, IFN, amino ac. metab. reactomes
WRNIP1_MTA3_RCOR1 [MTA3] CT CCTCCTCCCC	3,44	*Pou3f2*, *Nr1i3*, *Pou4f1_Pou6f1*, *Fgf21*, *G6pd*, *Cyp17a1* genes Ribosomal/RNA processes, Acetyl-CoA, triglyceride, serine synthesis, ECM, HIF pathways Glycolysis, IGF, triglyceride, collagen reactomes

Figures Captions

Fig.1. (A) Experimental procedures; (B) Cell morphology at the end of the experiments in control (CT) and biochips exposed to DDT150, PMT150 and Mix150; (C) and (D) collected cell number and albumin production in control and treated samples after 24 hours of exposition (72 hours of culture). The red arrows indicate the cell-free areas, *P < 0.05; **P < 0.01 (comparison with control, ANOVA one- way; Dunnett's test).

Fig.2. Transcriptome profiles: (A) and (B) PLS-DA score plots of all samples and CT vs. high-doses, respectively; (C) heatmap showing the variation in the top 5000 genes in transcriptome profile between CT and biochip treated with pesticides (DDT15, PMT15, Mix15, DDT150, PMT150 and Mix150).
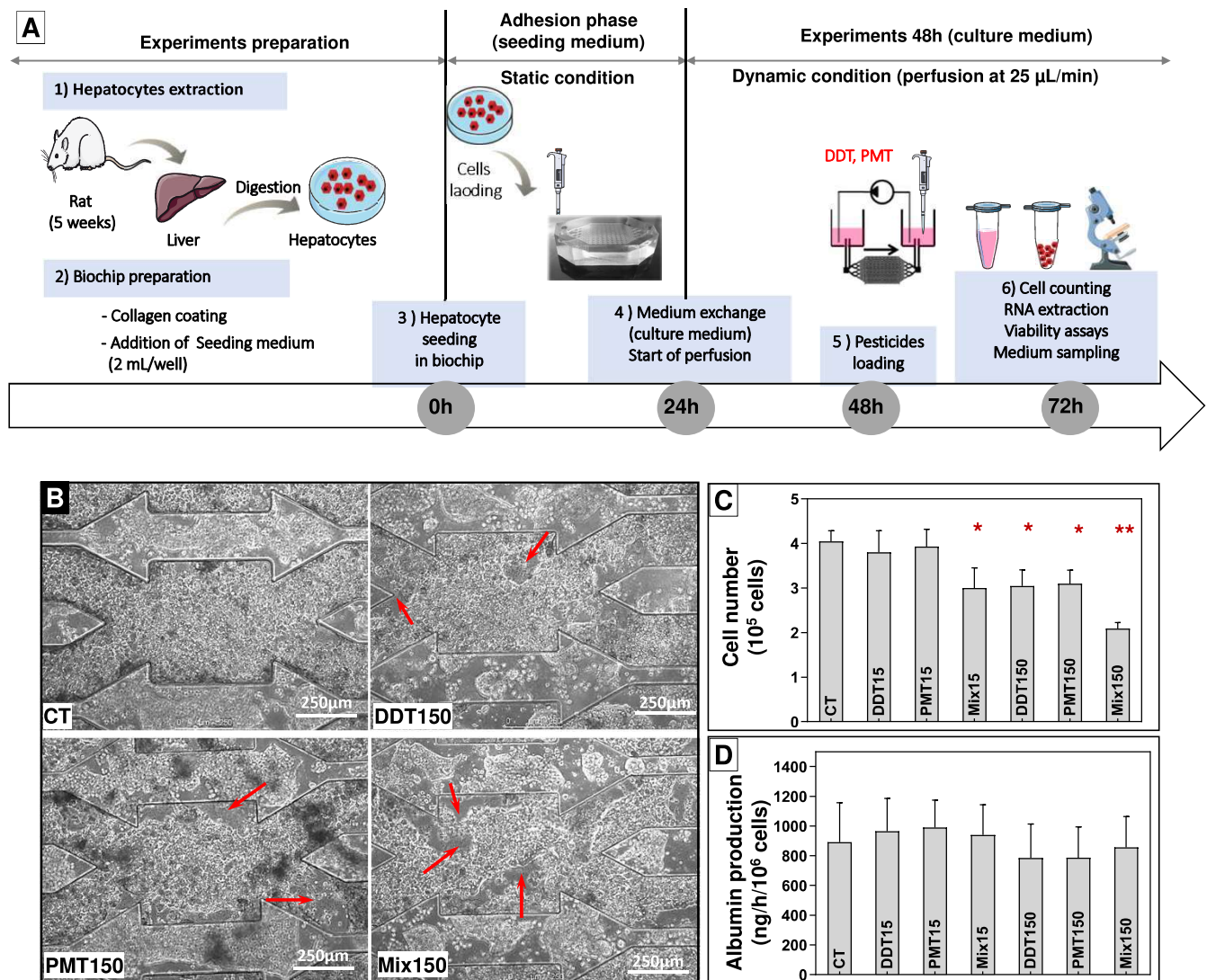
Fig.3. (A) Number of differentially expressed genes (GEGs) in biochips treated with DDT150, PMT150 and Mix150; (B) and (C) Venn diagram and correlation matrix analysis showing the correlation between transcriptome profiles of samples exposed to the pesticides high-doses (DDT150, PMT150 and Mix 150).
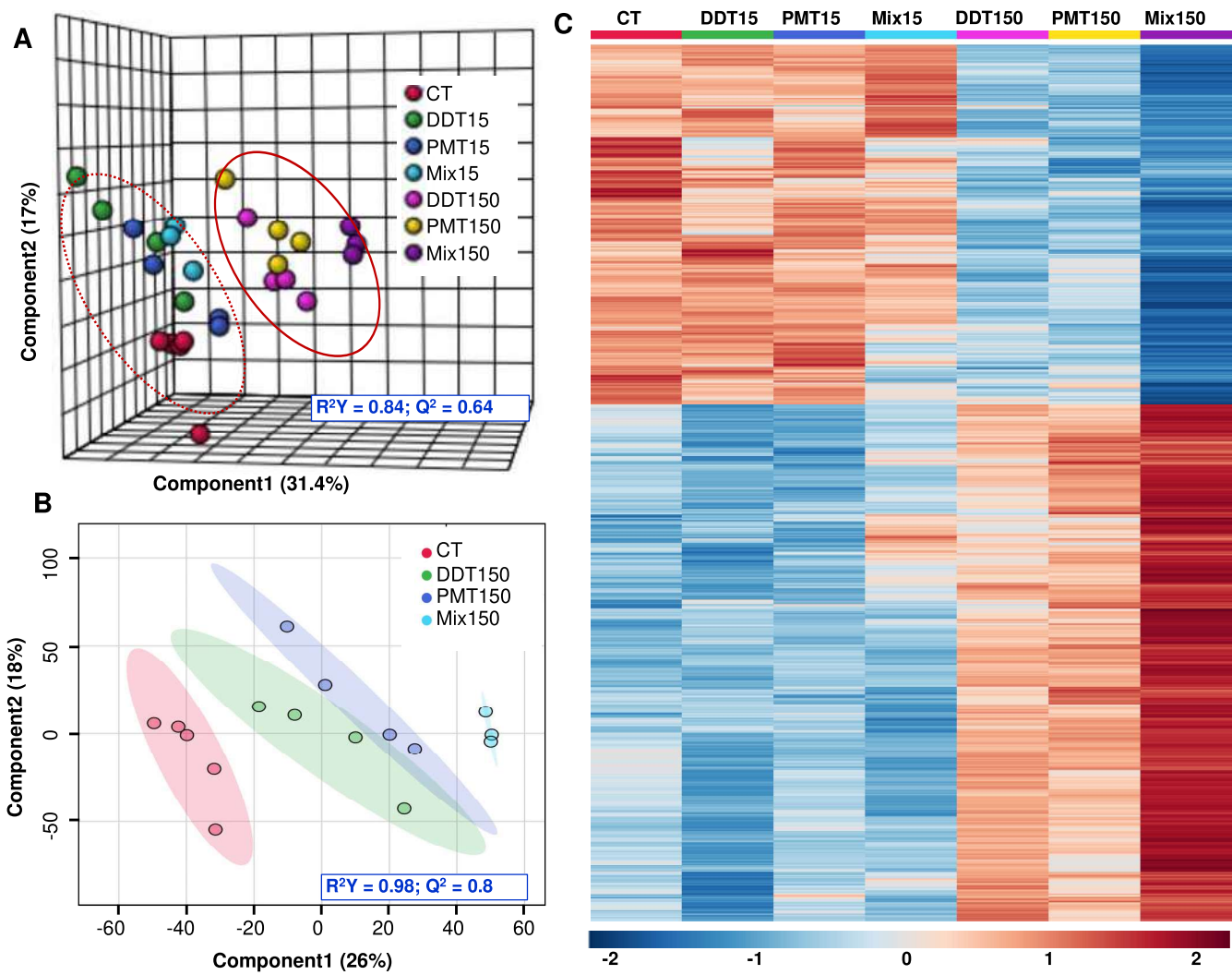
Fig.4. Metabolome profiles: (A), (B) and (C) OPLS-DA score plots of DDT150 vs. CT, PMT150 vs. CT and Mix150 vs. CT, respectively; (D), (E) and (F) S-plot from OPLS-DA analysis of DDT150 vs. CT, PMT150 vs. CT and Mix150 vs. CT, respectively (significantly modulated metabolites were selected based on p(corr) > 0.6, higher p[1] values and P < 0.05). Red and blue colors represent metabolites increased and decreased in treated samples. (1: tyrosine, 2: octanoic ac, 3: decanoic ac, 4: pyruvic ac, 5: glyceric ac, 6: fructose, 7: aspartic ac, 8: citric ac, 9: 2-hydroxybutyric ac, 10: cysteine, 11: allantoin, 12: glutamine, 13: valine, 14: leucine, 15: Ileucine, 16: lysine, 17: glutamic ac, 18: urea, 19: tagatose, 20: glucaric ac, 21: glycerol 3P, 22: A-alanine, 23: proline, 24: ornithine, 25: lactic ac, 26: glucose)
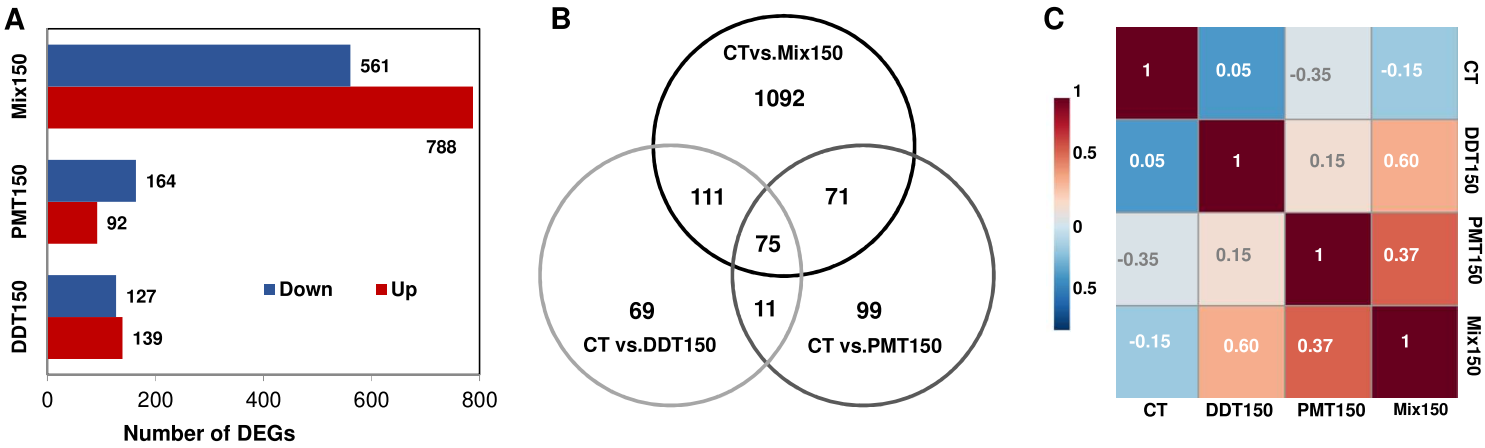
Fig.5. (A) Number of differentially expressed metabolites in biochips treated with DDT150, PMT150 and Mix150; (B) Venn diagram showing the correlation between metabolome profiles of samples exposed to the pesticides high-doses (DDT150, PMT150 and Mix 150); (C) heatmap showing the variation of differentially expressed metabolites between CT and biochip treated with pesticides DDT150, PMT150 and Mix150 (*P < 0.05; **P < 0.01 *P < 0.05; **P < 0.01
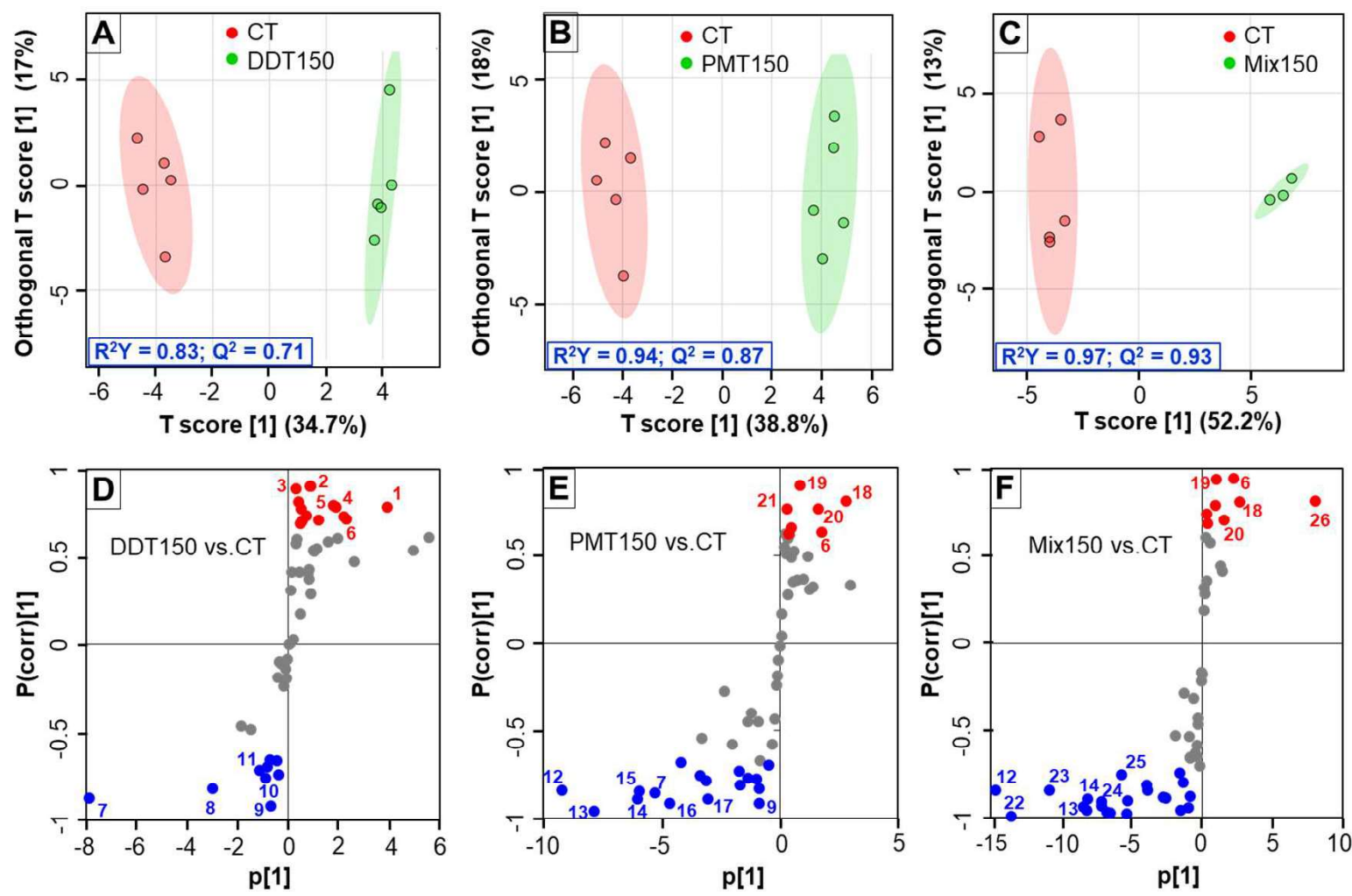
Fig.6. Results of pathway analysis performed using MetaboAnalyst software with the list of DEGs and discriminating metabolites: (A) DDT150 vs.CT; (B) PMT150 vs.CT and (C) Mix150 vs. CT. * Number of hits modulated in the pathway (1: central carbon
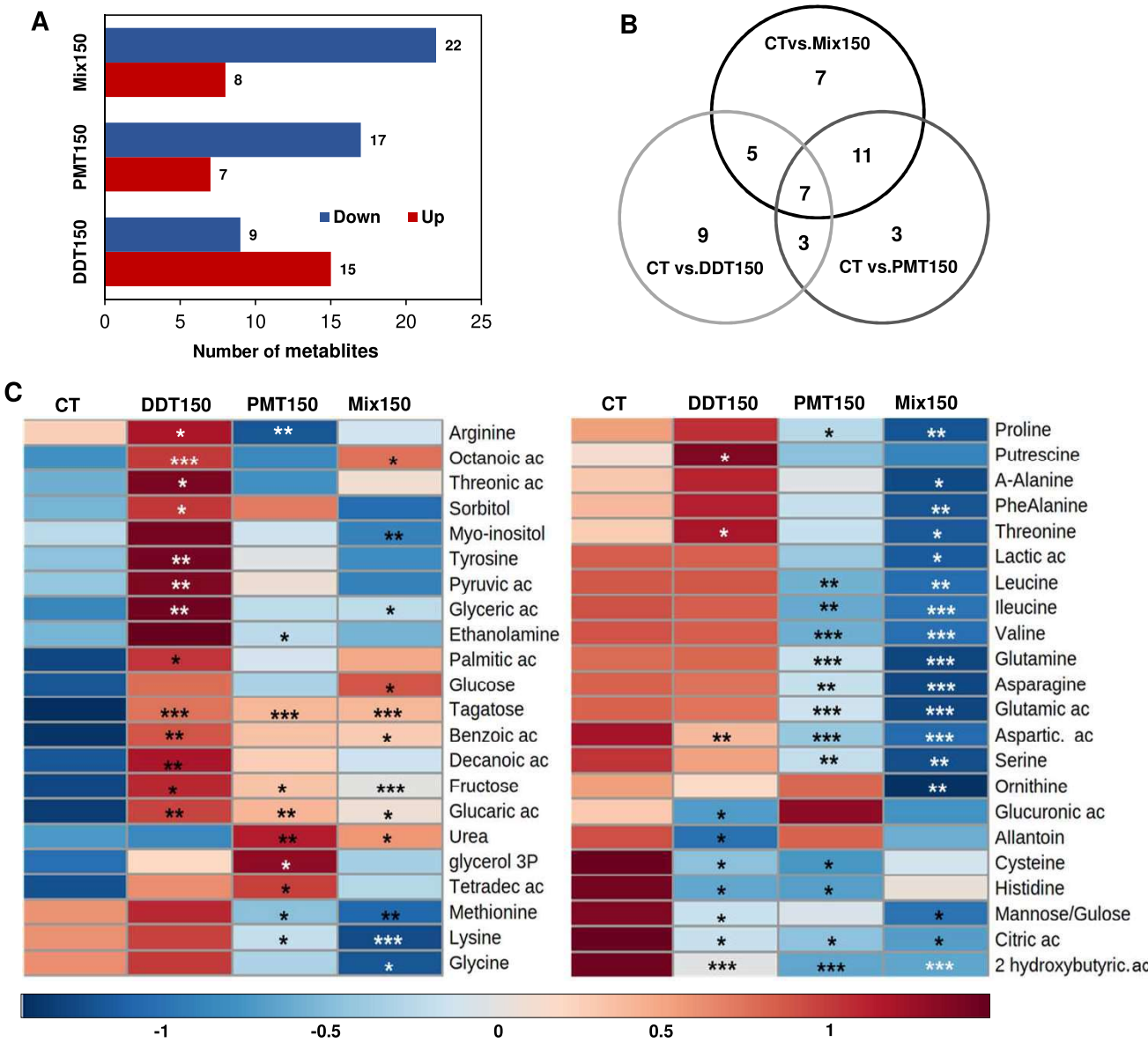
metabolism in cancer, 2: glycine, serine and threonine metabolism, 3: fatty acid biosynthesis, 4: PPAR signaling pathway, 5: fatty acid degradation, 6: necroptosis, 7: insulin resistance, 8: insulin signaling pathway, 9: aminoacyl-tRNA biosynthesis, 10: glycerolipid metabolism, 11: Arginine biosynthesis, 12: glucagon signaling pathway, 13: MAPK signaling pathway, 14: Glutathione metabolism).
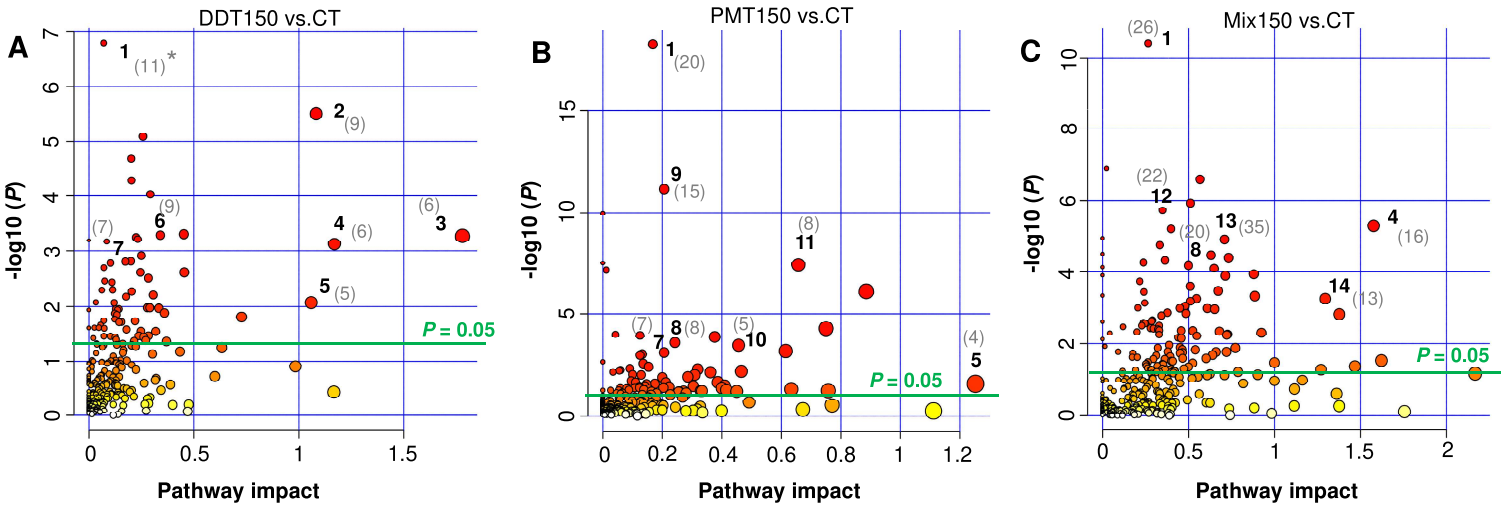
Figure1

Click here to access/download;Figure;Figure1.pdf ⬇

A Experiments preparation — Adhesion phase (seeding medium) — Experiments 48h (culture medium)

Static condition — Dynamic condition (perfusion at 25 µL/min)

1) Hepatocytes extraction

Rat (5 weeks) → Liver → Digestion → Hepatocytes

Cells loading

DDT, PMT

2) Biochip preparation
- Collagen coating
- Addition of Seeding medium (2 mL/well)

3) Hepatocyte seeding in biochip

4) Medium exchange (culture medium) Start of perfusion

5) Pesticides loading

6) Cell counting RNA extraction Viability assays Medium sampling

0h — 24h — 48h — 72h

B

CT   DDT150   250µm

PMT150   Mix150   250µm

C Cell number (10^5 cells)

CT, DDT15, PMT15, Mix15 *, DDT150 *, PMT150 *, Mix150 **

D Albumin production (ng/h/10^6 cells)

CT, DDT15, PMT15, Mix15, DDT150, PMT150, Mix150

Figure2

Figure3

Figure4

Click here to access/download;Figure;Figure4.pdf ⬇

Figure5

Figure6

Declaration of interests

☒ The authors declare that they have no known competing financial interests or personal relationships that could have appeared to influence the work reported in this paper.

☐The authors declare the following financial interests/personal relationships which may be considered as potential competing interests: